

Small emission sources in aggregate disproportionately account for a large majority of total methane emissions from the US oil and gas sector

James P. Williams¹, Mark Omara^{1,2}, Anthony Himmelberger², Daniel Zavala-Araiza¹, Katlyn MacKay¹, Joshua Benmergui^{1,2,3}, Maryann Sargent³, Steven C. Wofsy³, Steven P. Hamburg^{1,2}, Ritesh Gautam^{1,2}

¹Environmental Defense Fund, New York, NY, USA 10010

²MethaneSAT, LLC, Austin, TX, USA 78701

³Harvard University, Cambridge, MA, USA 02138

Correspondence to: James P. Williams (jamwilliams@edf.org), Ritesh Gautam (rgautam@edf.org)

Abstract. Reducing methane emissions from the oil and gas (oil/gas) sector has been identified as a critically important global strategy for reducing near-term climate warming. Recent measurements, especially by satellite and aerial remote sensing, underscore the importance of targeting the small number of facilities emitting methane at high rates (i.e., “super-emitters”) for measurement and mitigation. However, the contributions from individual oil/gas facilities emitting at low emission rates that are often undetected are poorly understood, especially in the context of total national- and regional-level estimates. In this work, we compile empirical measurements gathered using methods with low limits of detection to develop facility-level estimates of total methane emissions from the continental United States (CONUS) midstream and upstream oil/gas sector for 2021. We find that 70% (95% confidence intervals: 61-81%) of the total 14.6 (12.7-16.8) Tg/yr oil/gas methane emissions in the CONUS for the year 2021 originate from facilities emitting <100 kg/hr, and 30% (26-34%) and ~80% (68-90%) from facilities emitting <10 kg/hr and <200 kg/hr, respectively. While there is variability among the emission distribution curves for different oil/gas production basins, facilities with low emissions are consistently found to account for the majority of total basin emissions (i.e., range of 60% - 86% of total basin emissions from facilities emitting <100 kg/hr). We estimate that production well sites were responsible for 70% of regional oil/gas methane emissions, from which we find the well sites that accounted for only 10% of national oil and gas production in 2021, disproportionately accounted for 67-90% of the total well site emissions. Our results are also in broad agreement with data obtained from several independent aerial remote sensing campaigns (e.g., MethaneAIR, Bridger Gas Mapping LiDAR, AVIRIS-NG, and Global Airborne Observatory) across 5-8 major oil/gas basins. Our findings highlight the importance of accounting for the significant contribution of small emission sources to total oil/gas methane emissions. While reducing emissions from high-emitting facilities is important, it is not sufficient for the overall mitigation of methane emissions from the oil and gas sector which according to this study is dominated by small emission sources across the US. Tracking changes in emissions over time and designing effective mitigation policies should consider the large contribution of small methane sources to total emissions.

39 1 Introduction

40

41 Methane is a short-lived but powerful greenhouse gas with a global warming potential more than 80 times
42 stronger than carbon dioxide (CO₂) over 20 years (AR6 Synthesis Report: Climate Change 2023, 2024). Therefore,
43 the reduction of methane emissions has become a key goal to achieve rapid climate mitigation in the short term
44 (Ocko et al., 2021). In North America, one of the largest sources of methane emissions originates from the oil and
45 gas (oil/gas) sector, with most emissions originating from the production (i.e., upstream) and transportation/storage
46 (i.e., midstream) sectors (Alvarez et al., 2018). Multiple studies, especially over the past decade, have focused on the
47 quantification of methane sources from the oil/gas sector, with particular emphasis on the continental United States
48 (CONUS) (Alvarez et al., 2018; de Gouw et al., 2020; Omara et al., 2018; Lu et al., 2022; Zhang et al., 2020; Shen
49 et al., 2022; Cusworth et al., 2022; Nesser et al., 2023; Brandt et al., 2016; Duren et al., 2019; Maasackers et al.,
50 2021; Lu et al., 2023; Worden et al., 2022). Several studies have recognized the importance of a small percentage of
51 high-emitting sites (i.e. “super-emitters”) and reported them as accounting for a large fraction of total methane
52 emissions (Brandt et al., 2016; Cusworth et al., 2022; Duren et al., 2019; Sherwin et al., 2024). The emission rate
53 thresholds that characterize these super-emitting facilities are critical information for methane measurement
54 platforms, especially remote sensing technologies focused on detecting high-emitting point sources. Aerial and
55 satellite remote sensing technologies have enabled more frequent monitoring of emissions from oil and gas sites and
56 rapid mapping of large areas, although they face limitations in detection sensitivity. Despite the improved ability to
57 locate and quantify emissions from high-emitting sites, there has been considerable lack of understanding about the
58 characteristics of low methane emitting facilities, especially those emitting at rates below the limits of detection
59 (LOD) of most point-source detection remote sensing platforms, and their contributions to total oil/gas methane
60 emissions.

61 While some studies offer important yet limited insights into the contributions of different lower-emitting
62 infrastructure from the CONUS oil/gas sector, there is a lack of understanding about their overall contribution to the
63 total sectoral regional and national scale emissions. A recent study by Xia et al. (2024) combined aerial remote
64 sensing data from Bridger Gas Mapping LiDAR (Bridger GML) in four oil/gas basins supplemented with
65 component-level modeling for facilities emitting below the Bridger GML LOD and found significantly more
66 emission sources in the 1 – 10 kg/hr range when compared to the emission distribution used by the EPA (Xia et al.,
67 2024). In a study focused on production well sites in the CONUS, the main source of methane emissions from the
68 oil/gas sector (Alvarez et al., 2018; Omara et al., 2018; Rutherford et al., 2021), Omara et al. (2018) found that 90%
69 of total methane emissions from producing well sites came from those emitting at rates <100 kg/hr. A follow-up
70 study by Omara et al. (2022) highlights that the total methane emissions from low-producing well sites producing
71 less than 15 boe/day (i.e., 1 Mcf = 1,000 cubic feet of natural gas = 19.2 kg of methane at 15.6 °C and 1 atmosphere;
72 1 boe = 1 barrel of oil equivalent = 6 Mcf; assumed methane content in natural gas of 80%), which comprise 80% of

73 all producing well sites in the CONUS, were responsible for nearly half of all methane emissions from the oil/gas
74 production sector. Kunkel et al. (2023) observed that the use of the Bridger GML remote sensing platform with an
75 LOD of 3 kg/hr, combined with prior Carbon Mapper detections in a section of the Permian basin showed a
76 significant contribution from sources below the listed LOD of Carbon Mapper of 10 kg/hr. Cusworth et al. (2022)
77 found that 35% of total methane emissions (including non-oil/gas sources) from several major oil/gas producing
78 basins (other than the Appalachian basin) in the CONUS come from facilities emitting >10 kg/hr, indicating that
79 65% of emissions come from facilities emitting <10 kg/hr. Although these studies using independent measurement
80 platforms provide new emerging insights about the importance of low methane emitting oil/gas facilities, there
81 generally remains a lack of quantitative assessment of the relative fractions of emissions originating from different
82 emission rate thresholds aggregated over individual oil/gas basins as well as at a national scale.

83 There are a variety of different methane quantification methods that differ in terms of their spatial resolution of
84 sources, logistical constraints, costs of implementation, and their LODs. Measurement method sensitivities and
85 LODs have important policy implications. For example, the Environmental Protection Agency (EPA) recently
86 finalized regulations that define a “super-emitter event” as an emission rate threshold of 100 kg/hr or greater
87 (Standards of Performance for New, Reconstructed, and Modified Sources and Emissions Guidelines for Existing
88 Sources: Oil and Natural Gas Sector Climate Review, 2024), albeit without clear information on what percentage of
89 total regional emissions are captured within this definition. Satellite and aerial remote sensing methods have point
90 source LODs that range anywhere from 1-3 kg/hr for Bridger’s airborne GML (Johnson et al., 2021; Kunkel et al.,
91 2023; Thorpe et al., 2024; Xia et al., 2024) to ~200 kg/hr for GHGSat (Sherwin et al., 2023). In contrast, ground-
92 based measurement methods such as OTM-33a and tracer release have LODs <1 kg/hr (Fox et al., 2019). A study by
93 Ravikumar et al. (2018) using the Fugitive Emissions Abatement Simulation Toolkit (FEAST) suggests that a
94 method with a LOD of 0.1-1 kg/hr would sufficiently capture all emissions from the oil/gas sector, whereas the
95 ability to quantify emissions below this threshold would not lead to any significant increases in mitigation.
96 Ultimately, there is a need for clarification in the total percentage contribution of emissions originating from a given
97 emission rate threshold, which requires characterizing entire emissions distributions, not only the high emitters.

98 In this work, we create and analyze measurement-based methane emission rate distributions of US upstream and
99 midstream oil/gas facilities to determine the percentage contributions of different emission rate thresholds to total
100 methane emissions. First, we use empirical measurements gathered from ground-based sampling platforms to
101 develop a bottom-up facility-based model to estimate methane emissions for upstream and midstream facilities in
102 the continental US (CONUS) for 2021. Next, we aggregate our facility-level, population-based data to determine the
103 national- and basin-level contributions of methane emissions originating from facilities emitting at different
104 emission rate thresholds, in addition to comparisons to aerial-remote sensing platforms. Finally, we break down the
105 emission distribution curves by facility category to analyze how the percentage contributions of total emissions vary
106 across facility types.

107

108 **2 Materials and methods**

109

110 **2.1 Empirical measurements**

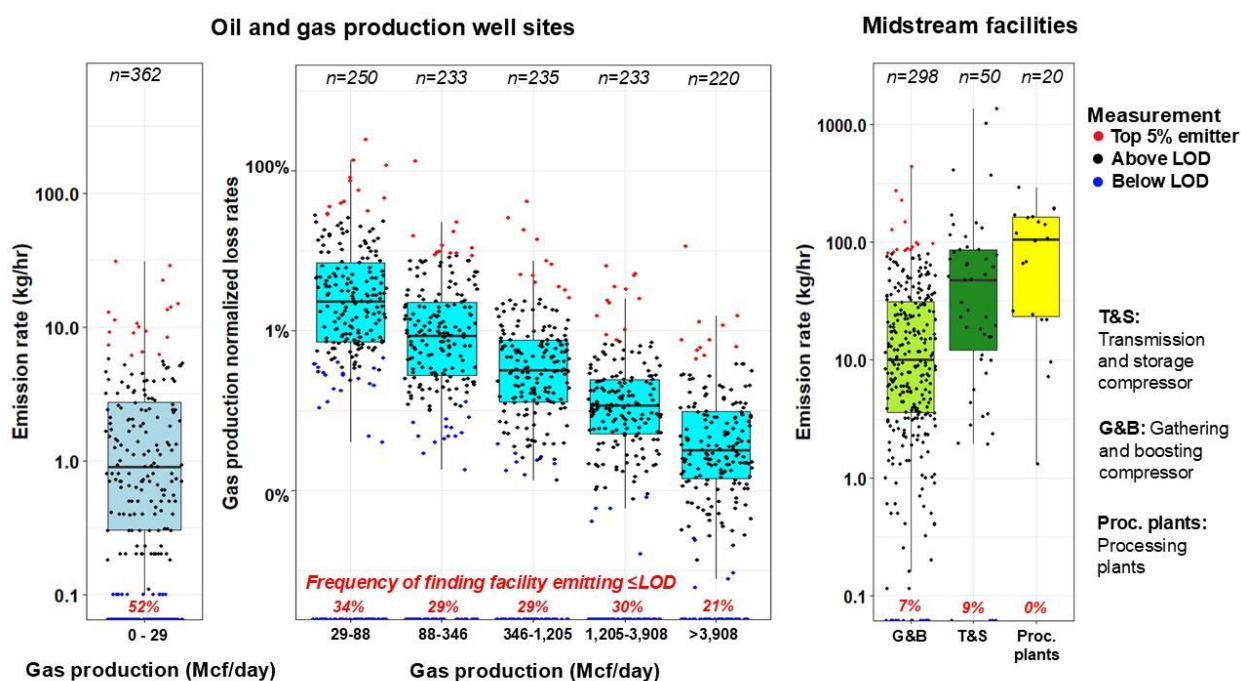
111

112 We compile 1,901 facility-level methane emission rate measurements from 16 studies (Brantley et al., 2014;
113 Caulton et al., 2019; Deighton et al., 2020; Goetz et al., 2015; Lan et al., 2015; Mitchell et al., 2015; Omara et al.,
114 2016, 2018; Rella et al., 2015; Riddick et al., 2019; Robertson et al., 2017, 2020; Subramanian et al., 2015;
115 Yacovitch et al., 2015; Zhou et al., 2021; Zimmerle et al., 2020) that use ground-based site/facility level and
116 source/component level measurement methods with low LOD's of ~0.1 kg/hr. Most (i.e., 85%) of empirical
117 measurements we use in this work were gathered using ground-based mobile laboratories that quantified methane
118 emissions at the site/facility level using either tracer-based releases, the EPA Other Test Method (OTM-33a), or
119 Gaussian plume transport modeling (Fox et al., 2019) (Table S2). The remaining 15% of empirical measurements we
120 use (Deighton et al., 2020; Riddick et al., 2019; Zimmerle et al., 2020) are ground-based methods that aggregated
121 source/component-level HiFlow sampling or static/dynamic chamber measurements, which could mean that other
122 on-site emission sources were not quantified during measurement and overall emission rate estimates are
123 conservative. Only one study was excluded from our analysis (ERG, 2011) due to a combination of age and a focus
124 on component-level measurements.

125 The compiled empirical measurements target a variety of production well sites and/or midstream facilities
126 across at least nine oil/gas-producing basins in the CONUS (Table S3). For all facility categories (i.e., production
127 well sites, gathering and boosting compressor stations, transmission and storage compressor stations, and processing
128 plants), we prioritize datasets of randomly sampled sites that include measurements below the method's LOD or
129 reported as zero emissions, except for measurements from two studies (Brantley et al., 2014; Lan et al., 2015) which
130 we discuss later in Section 2.3. Additionally, for production well site measurements, we focus only on data that
131 provide facility-level gas production data for the date/month of measurement. Our compiled dataset of
132 measurements includes both routine intentional (e.g., venting from pneumatic devices) and non-intentional (e.g.,
133 malfunctioning equipment and/or leaks from valves, connectors, flanges, etc) emissions, and while we remove any
134 measurements attributed to high emitting intermittent events such as flowbacks and liquids unloadings if that
135 information is present, we cannot fully discount that emissions from these high-emitting intermittent sources are
136 included in our compiled dataset. Furthermore, we remove any empirical measurement data associated with flaring
137 emissions, which are treated separately as discussed below, if that information is provided in the empirical data.

138 We categorize the empirical measurements by facility category as production well sites, gathering and boosting
139 compressor stations (G&B compressors), transmission and storage compressor stations (T&S compressors), or
140 processing plants. We group the empirical measurements from production well sites into six production bins based
141 on gross average daily gas production as reported in individual studies. We use gross daily average gas production
142 data instead of oil and gas production data for two reasons: 1) the limited availability of facility-level oil production
143 data provided from empirical measurement studies; and 2) the established relationship between gas production and

144 emission rates observed in previous work (Omara et al., 2018, 2022, 2024). The gas production ranges of the
 145 production bins (Fig. 1) are chosen to evenly distribute empirical measurements above the method LOD to all six
 146 production bins. This categorization creates nine distinct facility categories: G&B compressors, T&S compressors,
 147 processing plants, and six groups of production well sites. We further classify the nine distinct facility categories
 148 into five primary facility categories: low-production well sites which produce combined oil and gas <15 boe/day
 149 (i.e., 0.13 kt of methane production per year), non-low-producing well sites which produce ≥ 15 boe/day, processing
 150 plants, G&B compressors, and T&S compressors. In addition to these facility categorizations, we also include
 151 Visible Infrared Imaging Radiometer Suite (VIIRS) flare detections and flared gas volume estimates in our analysis,
 152 which are treated as an independent methane source since flares can be located on multiple facility categories across
 153 the upstream and midstream oil/gas sectors.



154

155 **Figure 1:** Facility-level empirical measurement data distributed by different distinct facility categories for production well sites
 156 (left) and midstream facilities (right). Individual measurements are shown for each box plot and colored according to their
 157 emission rate status for that facility category, where blue points are considered non-detectable emissions below an emission rate
 158 threshold of ≤ 0.1 kg/hr/facility which is the method LOD we use, black points are measurements above our method LOD but
 159 below the top 5% emitter category, and red points are the top 5% of empirical emission rates or loss rates for that facility
 160 category. The number of empirical measurements available for each facility category is denoted at the top of each boxplot. The
 161 estimated mean frequency of finding a facility emitting below the method LOD is shown in inset red text at the bottom of each
 162 boxplot. We show absolute emission rates (kg/hr) rather than normalized loss rates (%) for the lowest cohort of production well
 163 sites due to the reasoning presented in Section 2.3. Unit conversions: 1 Mcf = 1,000 cubic feet of natural gas = 19.2 kg of
 164 methane at 15.6 °C and 1 atmosphere; 1 boe = 1 barrel of oil equivalent = 6 Mcf; assumed methane content in natural gas of 80%.

165

166 2.2 Activity data

167

168 We use activity data (i.e., number of facilities and spatial locations) for actively producing wells in 2021
169 provided by Enverus for the CONUS. We calculate both the annual averaged daily gross gas production, and oil and
170 gas production for each producing well using the number of producing days and total annual oil and gas production
171 data provided by Enverus. We convert production wells to production well sites by spatially aggregating individual
172 wells within 25-meter (vertical wells) or 50-meter (horizontal wells) distances from each other and separately
173 merging their combined oil and gas production and gas production, and converting these production values to a mass
174 equivalent production rate in kg/hr of methane (i.e., 1 Mcf = 1,000 cubic feet of natural gas = 19.2 kg of methane at
175 15.6 °C and 1 atmosphere; 1 boe = 1 barrel of oil equivalent = 6 Mcf; assumed methane content in natural gas of
176 80%), similar to previous approaches (Omara et al., 2018).

177 We acquire activity data for operational transmission and storage (T&S) and gathering and boosting (G&B)
178 compressor stations and processing plants from Enverus for 2021 for the CONUS, which was further supplemented
179 by additional data from the Oil and Gas Infrastructure Mapping (OGIM) database published in Omara et al. (2023).
180 We filter data for these midstream facilities to include only active facilities in the year 2021. For VIIRS flare
181 detections, we use the 2021 natural gas flared volume estimates based on natural gas flaring detections provided by
182 the VIIRS instruments installed aboard satellite platforms which have a 750x750 meter source resolution (NOAA-20
183 and Suomi National Polar-orbiting Partnership) (Elvidge et al., 2015). In terms of potential double-counting between
184 the VIIRS flare detections and the empirical measurements we use in this work, the majority of VIIRS detections are
185 in the Permian, Bakken, and Eagle Ford oil/gas basins (i.e., 86% of total VIIRS detections) which corresponds to a
186 small number of our empirical measurement data (Table S3) (Plant et al., 2022). However, the limited availability of
187 spatial coordinates for our empirical measurements restricts our ability to perform a direct comparison to exclude
188 overlapping/proximal VIIRS detections and our facility-level empirical measurements. Therefore, we do
189 acknowledge that there is a possibility of double counting between our empirical measurement data and the VIIRS
190 flare detections, but we expect the degree of overlap to be low.

191 **2.3 Facility-level methane emission inventory**

192 We calculate annual methane emissions from all facility categories (i.e., six production bins of production well
193 sites, T&S compressor stations, G&B compressor stations, processing plants, and VIIRS flare detections) using a
194 multi-step probabilistic modeling approach adapted from multiple studies (Omara et al., 2018, 2022; Plant et al.,
195 2022) (Fig. 2). Briefly, for each individual facility and VIIRS flare detection in the CONUS for 2021, we estimate an
196 annually averaged methane emission rate using empirical measurement data, and consequently the cumulative
197 distribution of methane emission rates from the aggregation of these individual emission rates. Each emission rate
198 estimate is indexed according to the corresponding replicate (n=500), and we use these repetitions to determine
199 uncertainty for the cumulative methane emission distribution curves. The detailed steps of this process for all facility
200 categories and VIIRS flare detections are described below.

201 For the highest five gas production bins of producing well sites ranging from 29 to >3,908 Mcf/day (or 0.2 to
202 >27 kt of methane production per year, Figure 1), we use gross gas production normalized loss rates to model the

203 distributions used to calculate methane emission rates from Eq. (1), where the: *Loss rate* is the fraction of emitted
 204 gas relative to gas production, the *emission rate* is rate of methane emitted from a facility in kilograms per hour,
 205 σ_{CH_4} is the methane content of the emitted gas which we assume to be 80%, and the *gas production* is the mass
 206 equivalent of natural gas produced in kilograms per hour at 1 atmosphere and 15.6 °C (1 Mcf = 1,000 cubic feet of
 207 natural gas = 19.2 kg of methane at 15.6 °C and 1 atmosphere; 1 boe = 1 barrel of oil equivalent = 6 Mcf). For the
 208 lowest well site gas production bin of 0 to 29 Mcf/day (i.e., 0 to 0.2 kt of methane production per year) and
 209 midstream facilities, we use the empirical absolute methane emission rate data as is. This approach is partly based
 210 on the methods used by Omara et al. (2022) for the low production well site category, which exploits a weak
 211 relationship between gross gas production data (which is most accessible in empirical measurement studies) and
 212 absolute emission rates to better extrapolate emissions to the entire population of production well sites in the
 213 CONUS.

$$214 \quad Loss\ rate = \frac{Emission\ rate\ \left[\frac{kg}{hr}\right]}{\sigma_{CH_4} \times Gas\ production\ \left[\frac{kg}{hr}\right]} \quad (1)$$

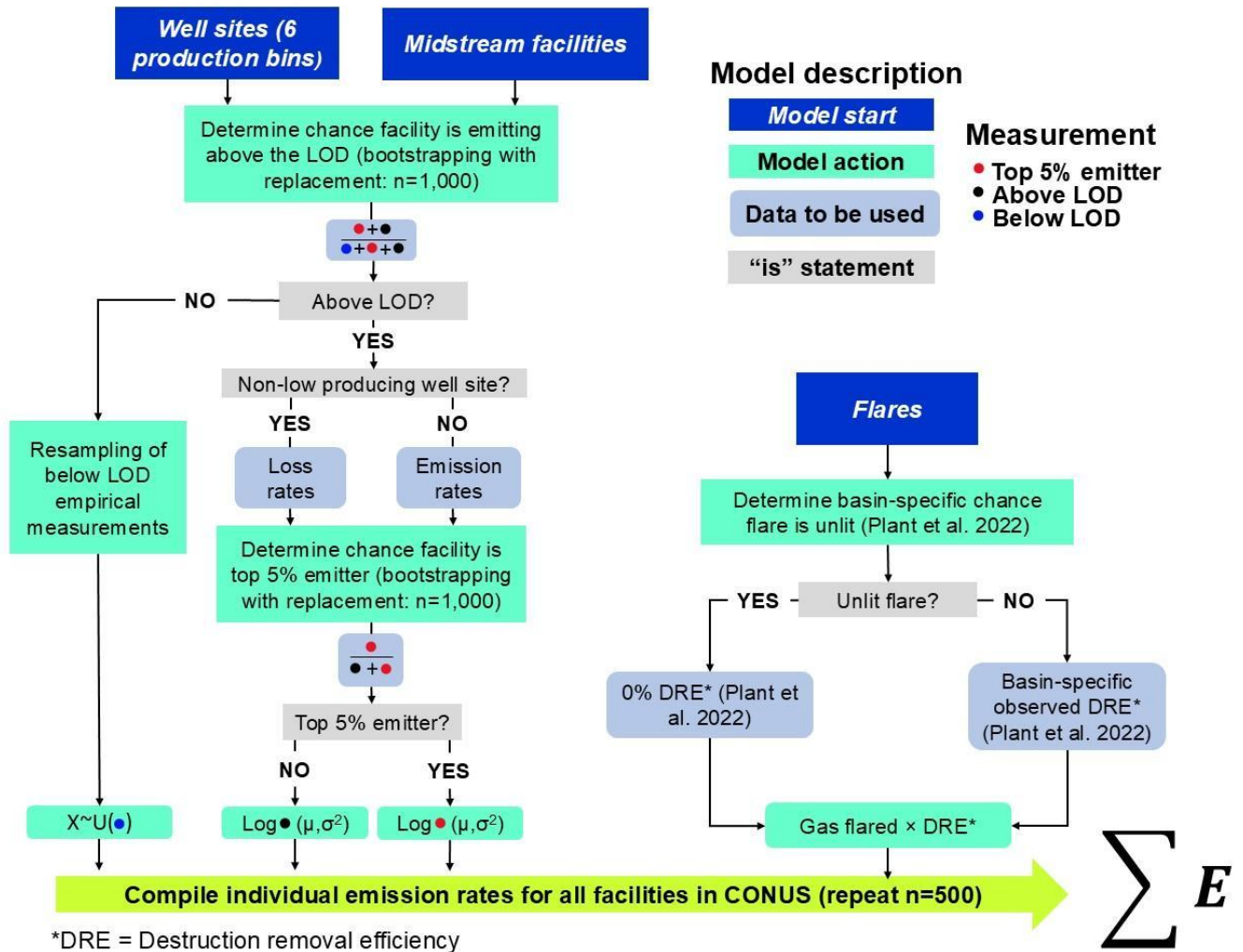
215 For our estimation of facility-level emission rates, we break down the modeling process into two separate steps:
 216 the first determines whether a randomly selected facility is emitting methane above our method LOD of ≤ 0.1
 217 kg/hr/facility, and the second determines the associated methane emission rate for that individual facility. To test the
 218 sensitivity of our method to the selection of the method LOD, we also perform an additional sensitivity analysis for
 219 other method LODs (Fig. S8). The processes outlined below are all specific to each of our nine facility categories.
 220 Brantley et al. (2014) and Lan et al. (2015) are excluded from this first step since they do not include measurements
 221 below the method LOD but include valuable data on well site emission rates with associated well site production
 222 data. To determine whether a facility is emitting methane above the method LOD threshold in our estimates, we first
 223 use bootstrapping with replacement (n=1,000) of our empirical measurement data to simulate the frequency of
 224 finding an individual facility emitting methane above the method LOD (i.e., ≤ 0.1 kg/hr/facility), which we call an
 225 “emitting facility” or “emitter” herein (Fig. 2). The results of the bootstrapping procedure represent a normal
 226 probability distribution from which we estimate the frequency of finding an emitting facility (i.e., above the method
 227 LOD) with associated uncertainty bounds. Next, we remove the empirical measurements below the LOD and use
 228 bootstrapping with replacement (n=1,000) on the above LOD empirical measurements to determine the probability
 229 of an emitting facility being in the top 5% (i.e., 95th percentile or above of empirical measurement data) or bottom
 230 95% (i.e., 95th percentile or below the empirical measurement data) of emitters, except for processing plants and
 231 T&S compressors which had too few measurements (n=20 and n=50 respectively) to distinguish between the top 5%
 232 and bottom 95% of emission or loss rates. Similar to the process of determining the frequency of finding an emitting
 233 facility, we use the results of the bootstrapping to develop a normal probability distribution that classifies an
 234 emitting facility as either a top 5% or bottom 95% emitter. This pseudo-random selection of a top 5% emitter within
 235 each facility category accounts for the functional definition of abnormally large emissions (i.e., super-emitters) that
 236 can be observed in all facility categories (including well sites in different production bins) (Zavala-Araiza et al.
 237 2015, Brandt et al. 2016). We fit the results of the bootstrapping to two normal distributions: one for the top 5% of

238 emitters and one for the bottom 95% of emitters. We use the associated parameters of each normal distribution to
239 randomly determine whether a facility is emitting in the top 5% or bottom 95% of emitters. These steps are repeated
240 for each facility for each facility category in the CONUS.

241 At the end of the first step of this facility-level modeling process, all facilities in the CONUS are classified as
242 either a: bottom 95% emitter, top 5% emitter, or below the method LOD. Loss rates are used to calculate emission
243 rates for the top five highest production bins of well sites, whereas we directly estimate methane emission rates for
244 the well sites in the lower production cohort (Fig. 1), and for midstream facilities excluding VIIRS flare detections.
245 For facilities classified as the top 5% and bottom 95% of emitters, we estimate their methane emissions by first
246 fitting a lognormal distribution to the empirical measurement data, including measurements from Brantley et al.
247 (2014) and Lan et al. (2015), of either the gas production normalized loss rates or methane emission rates (Eq. 1),
248 depending on the facility category. Next, we use the parameters of the modeled distributions to randomly assign
249 either an emission or loss rate to a randomly selected facility (n=500), depending on its emitter status and facility
250 category. We test each estimated methane emission distribution to the associated empirical measurements and find a
251 good fit for all facility categories (Table S6). To account for facilities emitting below the method LOD, we
252 randomly assign an emission rate from re-sampling our dataset of empirical measurements below the method LOD
253 for that facility category. Finally, once all facilities are assigned an emission rate, we compile the ensemble of
254 emission distributions to develop facility-level emission distribution curves and total regional oil/gas methane
255 emissions for the CONUS in 2021.

256 For all VIIRS flares detections, we use the total reported volumes of gas flared for 2021 from flares detected
257 using the VIIRS instrument (Elvidge et al. 2015) multiplied by the observed flare destruction efficiencies and
258 percentage of unlit flares from Plant et al. (2022) to calculate annual methane emission rates from this source. As
259 previously stated, our empirical measurements are largely located outside of oil/gas basins where the majority of
260 VIIRS flare detections are located (i.e. Permian, Eagle Ford, and Bakken), but we cannot discount the possibility
261 that there are instances of double-counting flares measured via our ground-based empirical data and those detected
262 by VIIRS. For each VIIRS flare detection, we randomly determine whether it is an unlit or lit flare based on the
263 basin-specific percentages of unlit flares reported by Plant et al. (2022). If a flare is determined to be lit, we use the
264 corresponding basin-specific observed destruction removal efficiencies as reported by Plant et al. (2022) multiplied
265 by the corresponding annual total volume of gas flared and convert to an emission rate. The basin-specific observed
266 destruction removal efficiencies are estimated through a fitted normal distribution using the mean and standard
267 deviations modeled from the 95% confidence intervals presented in Plant et al. (2022). If a flare is determined to be
268 unlit, we use a destruction removal efficiency of 0%. For VIIRS flare detections located outside of the Bakken,
269 Eagle Ford, and Permian basins, we used the total CONUS averaged destruction removal efficiencies of 95.2%
270 (95% confidence interval: 94.3 – 95.9%) and percentage of unlit flares of 4.1% as reported by Plant et al. (2022).

271



272

273

274

275

276

Figure 2: Flowchart describing the facility-level estimates, with steps colored according to the specific process and data being used. We note that methane emission rates for flares are calculated using a separate approach from that of production well sites and midstream facilities. Processing plants and T&S compressors are excluded from the determination of whether a facility is a top 5% emitter due to a lack of available empirical measurement data.

277

278

279

2.4 Extrapolation to smaller spatial boundaries

280

281

282

283

284

285

286

287

We perform several comparisons of our estimated emission distribution curves and total aggregated emissions to estimates from aerial and satellite remote-sensing studies. To perform these comparisons, we restrict our estimates and the results from other aerial/satellite studies to spatial domains of interest (e.g., an oil/gas basin boundary or the overflow domain from an aerial sampling campaign), and to specifically compare estimates of oil/gas methane emissions from the facility categories we are investigating in this work. For comparisons to satellite remote-sensing studies, we prioritize national-level satellite inversions that estimate methane emissions from the CONUS that include spatially explicit maps of methane emission inversions specifically for oil/gas sources. We join the spatially explicit satellite inversions of methane emissions to the top twelve producing oil/gas basin boundaries

288 in the CONUS, in addition to their national-level inversions which we also use for national comparisons. Since our
289 facility-level model includes geo-located activity data (i.e., facility coordinates), we can estimate facility-level
290 methane emissions distributions and estimate total methane emissions for any spatial boundary in the CONUS by
291 spatially joining facilities within a target boundary. Spatial variability in our facility-level estimates is driven by two
292 main factors: counts of facilities and facility types, and averaged annual production characteristics. Due to
293 constraints on data availability, we do not constrain our available empirical measurement data to the specific regions
294 where they were gathered (Table S3). We tested the sensitivity of excluding empirical measurements gathered from
295 specific oil/gas on the national emission distribution curves and total national methane emissions and found no
296 significant variation (Fig. S9). Due to a lack of data availability, we do not have sufficient spatial information from
297 empirical measurements of G&B compressors, T&S compressors, and processing plants to test for basin-level
298 differences in empirical measurement data.

299 For comparisons to aerial remote sensing studies/results, we prioritize studies that include both measured
300 point sources (i.e., oil/gas methane sources that are above the LOD of the aerial remote sensing measurement
301 platform), estimates of total regional oil/gas emissions, and descriptions/outlines of the surveyed spatial domains
302 which are required for these comparisons. Based on these criteria, we compare our estimated emissions to those
303 from peer-reviewed studies (Cusworth et al., 2022; Kunkel et al., 2023; Xia et al., 2024) and the results of research
304 flights from MethaneAIR in the Permian and Uinta oil/gas basins (Omara et al., 2024; Chan Miller et al., 2023;
305 Chulakadabba et al., 2023; MethaneAIR, 2024), with discussion in later sections on a recent study by Sherwin et al.
306 (2024). In all cases, we estimate facility-level methane emissions within the spatial domains outlined by the aerial
307 remote sensing studies to estimate region-specific methane emission distribution curves, use the relevant method
308 limits of detection to characterize emission rate thresholds valid for comparison, and subtract any emission unrelated
309 to the facility types we characterize (Chen et al., 2024). In the case of Cusworth et al. 2022, we infer the spatial
310 domains by georeferencing figures from their studies using the georeferencer tool QGIS (v.3.34.2-Prizen). We
311 compare our spatially joined facility-level emission distributions to the percentage of emissions contributed from
312 facilities emitting below discrete methane emission rate thresholds for all four aerial remote sensing studies, and to
313 the continuous cumulative methane emissions distribution curves from Bridger GML surveys (Kunkel et al., 2023;
314 Xia et al., 2024).

315 Each aerial remote sensing campaign utilizes independent methods to estimate their percentage
316 contributions from small methane sources, which in some cases requires additional analysis of the aerial remote
317 sensing results. For our analysis of continuous methane emissions distribution curves from the Bridger GML
318 campaigns (Kunkel et al., 2023; Xia et al., 2024), we restrict our analysis to estimated emission rates >3 kg/hr,
319 which is the approximate LOD of the Bridger GML remote sensing platform. For MethaneAIR, we use the
320 percentage of area emissions (i.e., diffuse area methane sources) relative to the total methane emissions for the
321 spatial boundary, which roughly corresponds to all emissions <200 kg/hr (i.e. effectively those emissions below the
322 point source detection limit of MethaneAIR that flew in multiple campaigns in the US at 40,000ft above ground
323 level (Chulakadabba et al., 2023)). MethaneAIR characterizes the total regional emissions including the spatial area

324 emissions at high resolution using a geostatistical inverse modeling framework (Miller et al., 2013) while ingesting
325 high-emitting point source information in the inversion (Chulakadabba et al., 2023; Omara et al., 2024). For
326 Cusworth et al. (2022), we analyze all campaigns by subtracting both aerially detected pipeline emissions and all
327 non-oil/gas emissions (e.g., wastewater, landfills, agriculture), since our study is focused solely on upstream and
328 midstream oil/gas sources. In addition, we subtract emissions from pipelines and non-oil/gas sources emitting below
329 aerial detection limits (i.e., TROPOMI inversions subtracted by aerially detected emissions) by estimating the
330 relative fractions of pipeline and non-oil/gas sources from the aerial detections, with the assumption that these
331 fractions are representative (Table S4). However, this process can introduce additional uncertainties in our
332 comparisons, especially for campaigns where 50% or more of aerially detected emissions were from pipelines or
333 non-oil/gas sources.

334 We account for the intermittency of detected methane sources with <3 overpasses in Cusworth et al.
335 (2022) by resampling with replacement ($n=1,000$) the source persistence of methane sources with ≥ 3 overpasses for
336 the same campaign, which is consistent with their methodology. We calculate the percentage contributions of low
337 emitting sources in Cusworth et al. (2022) using Eq. (2): where $\%E_{<x}$ is the percentage of total oil/gas methane
338 emissions below an emission rate threshold x (kg/hr), T is the total area emissions measured via TROPOMI
339 inversions (kg/hr), and $P_{>x}$ is the sum of point source emissions above the emission rate threshold x (kg/hr).

$$340 \quad \%E_{<x} = 1 - \frac{P_{>x}}{T} \quad (2)$$

341 2.5 Uncertainty calculations

342

343

344 Our emission distributions based on facility-level estimates incorporate uncertainty through several steps, such
345 as the: probabilistic distributions of a select facility being a top 5%, bottom 95% emitter, or facility emitting below
346 the LOD; emission rate and loss rate distributions produced from facility-level empirical measurements; and flaring
347 combustion efficiencies. In addition, we incorporate uncertainties from the empirical measurements into our facility-
348 level model by simulating new empirical emission rates based on the associated method uncertainties. At the
349 beginning of each of the 500 model iterations, we use the reported empirical methane emission rate data and
350 estimate a new emission rate using a normal distribution with the mean as the initial reported emission rate and the
351 standard deviation as a percentage of the mean value. These measurement uncertainties (i.e., 1-sigma) are chosen
352 based on the measurement methodology using the lower percentage uncertainty ranges provided by Fox et al. (2019)
353 for facilities measured via the OTM-33a ($\pm 25\%$), Gaussian plume dispersion ($\pm 50\%$), and tracer release ($\pm 20\%$)
354 methods. For HiFlow sampler measurements, we use an uncertainty range of $\pm 16\%$ (Riddick et al., 2022), and for
355 chamber-based measurements, we use $\pm 14\%$ (Williams et al., 2023). Therefore, each model iteration incorporates a
356 unique suite of empirical measurement data based on the initially reported emissions and their associated
357 uncertainties, which in turn impacts the probabilistic modeling of the chance of a facility emitting below the method
358 LOD, the empirical data is used to determine the parameters of the lognormal distributions of loss rates and emission

359 rates, and the ranges of the production bins. To calculate the cumulative uncertainty of our facility-level model
360 estimates, we estimate 500 methane emission distributions and aggregate the 2.5th and 97.5th percentiles of our seven
361 primary facility categories (i.e., low and non-low producing well sites, G&B compressors, T&S compressors, and
362 processing plants), which include lit and unlit VIIRS flare detection emissions, to determine our 95% confidence
363 intervals. This process is repeated for all simulations at the national-, basin-, and aerial remote sensing boundary
364 levels. For uncertainty calculations in satellite- and aerial-remote sensing studies we use for comparisons, we present
365 the reported 95% confidence intervals, if available.

366

367 **3 Results**

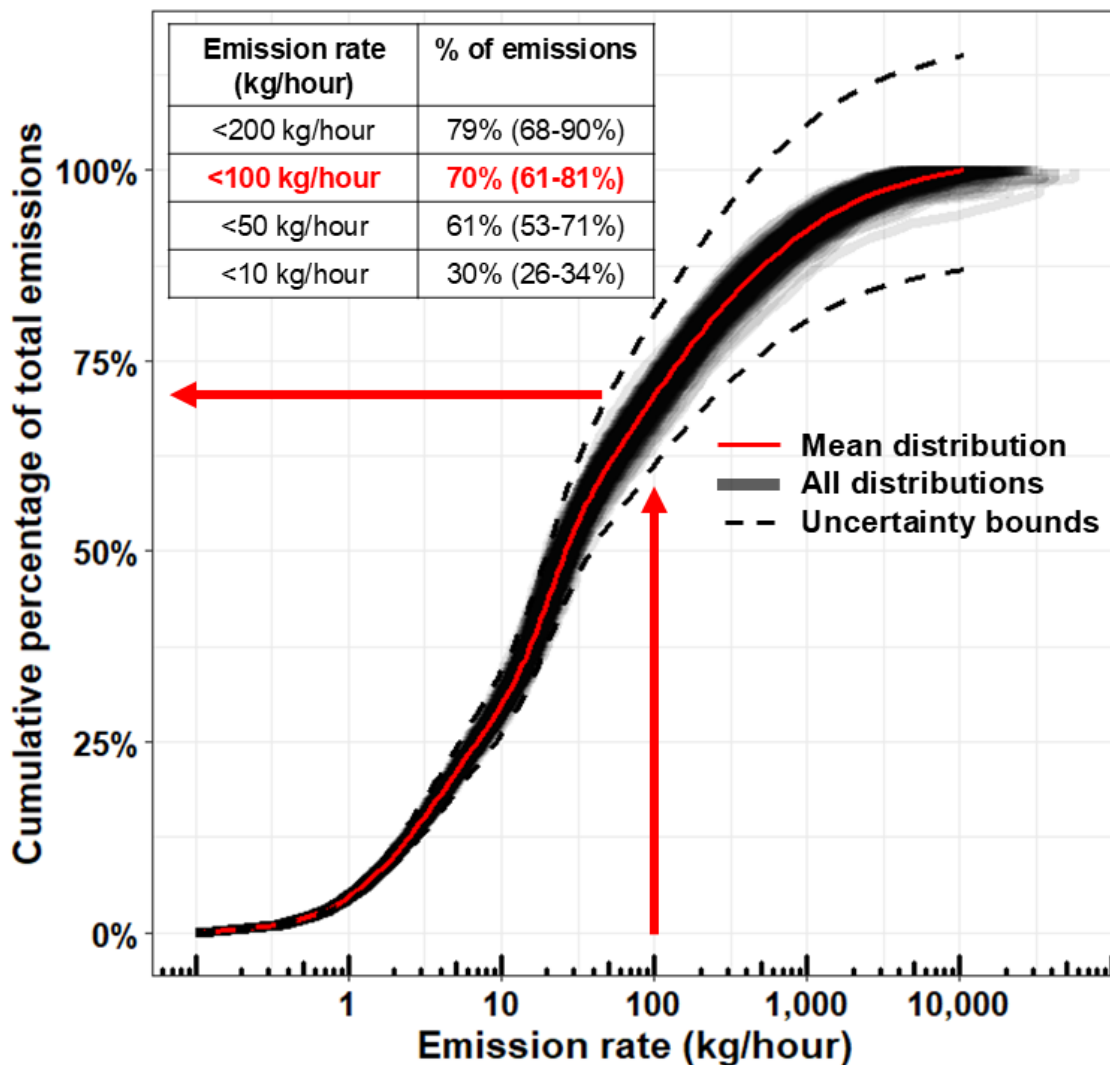
368

369 **3.1 Distribution of emission rates at the national scale**

370

371 Based on the results from our facility-level model estimates, we estimate that 70% (95% confidence
372 interval: 61-81%) of total methane emissions from the upstream/midstream sector in the CONUS for 2021 originate
373 from facilities emitting methane at rates <100 kg/hr (Fig. 3). For other emission rate thresholds, we find that 30%
374 (26-34%) of total emissions come from facilities emitting <10 kg/hr, which corresponds to the lower thresholds of
375 aircraft-based aerial remote sensing studies (Cusworth et al., 2022; Johnson et al., 2021; Kunkel et al., 2023; Thorpe
376 et al., 2024; Xia et al., 2024), and 79% (68-90%) of total emissions come from facilities emitting <200 kg/hr. We
377 find that the emission rate threshold corresponding to 50% of cumulative methane emissions from
378 upstream/midstream facilities in the CONUS for year 2021 is 25 kg/hr (19-33 kg/hr). These results suggest that a
379 large majority of oil/gas emissions in the CONUS are not detectable by existing satellite remote-sensing point

380 source imagers (Sherwin et al., 2023).



381

382 **Figure 3:** Results from 500 estimated facility-level emission distributions showing the cumulative percentages of
383 total methane emissions contributed from facilities emitting below methane emission rate thresholds. For example,
384 facilities emitting <100 kg/hr account for 70% (61-81%) of total methane emissions. The inset table in the upper left
385 displays the total percentage of methane emissions contributed from several discrete emission rate thresholds with
386 95% confidence intervals shown in parenthesis.

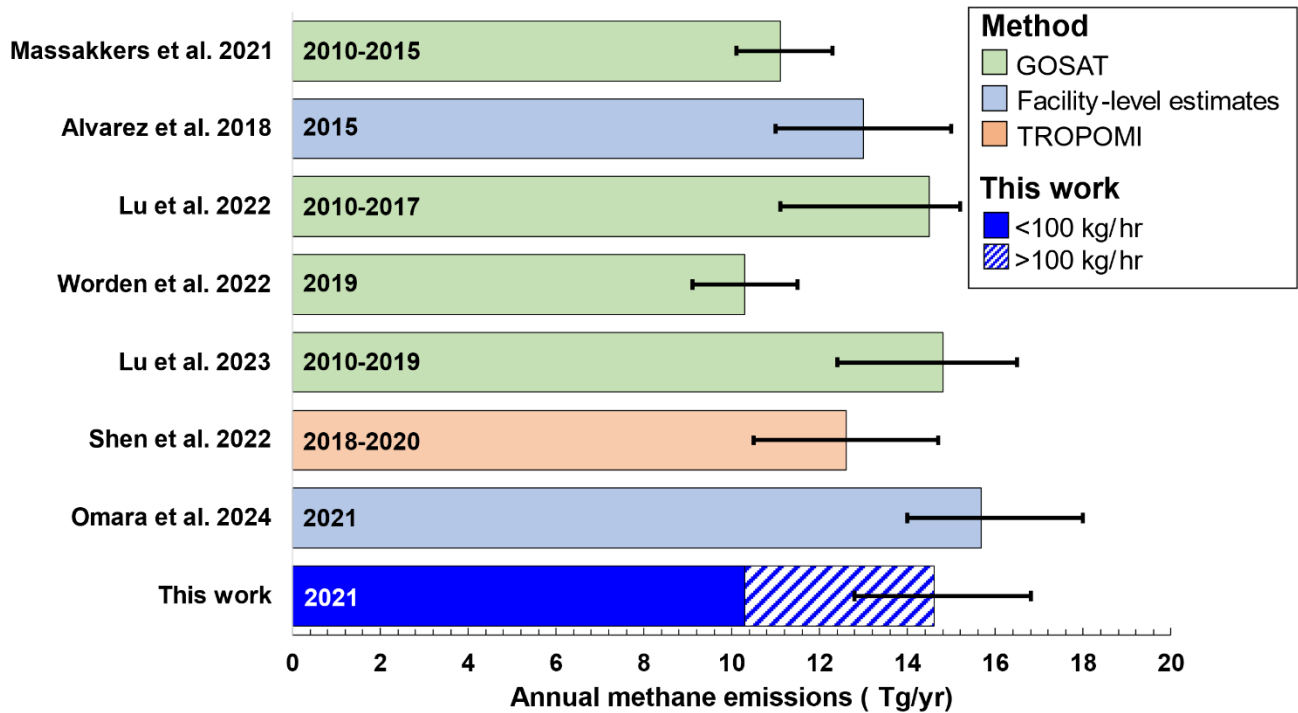
387

388 The distribution for our national-level methane emissions follows an S-shaped curve, noting that the x-axis
389 (i.e., facility-level methane emission rates) is presented in the \log_{10} scale. From 0.1 to 1 kg/hr, we observe a plateau
390 in the distribution curve indicating that increasing emission rates within this range do not significantly increase the
391 percentage contribution to total regional emissions (Fig. 3), similar to the findings in Ravikumar et al. (2019). From 1
392 to 100 kg/hr, we see a sharper rise in the emission distribution, indicating that increasing emission rates at this range
393 lead to a more substantial contribution to total methane emissions, and account for 68% (60 – 75%) of total methane

394 emissions (Fig. 3, Table S4). Above an emission rate threshold of 100 kg/hr, we see an exponential decline in the
395 percentage contributions of total emission with increasing emission rates, with total methane emissions in this range
396 amounting to 28% (18 – 37%) of the total oil/gas emissions. Facilities emitting at the 1-10 kg/hr and 100-1,000 kg/hr
397 ranges contribute a similar cumulative percentage at 26% (23 - 29%) and 22% (18 - 26%) respectively. Similar
398 percentage contributions are also observed between the 0.1-1 kg/hr and >1,000 kg/hr ranges at 4.5% (4.0 - 5.1%) and
399 6.1% (2.6 - 13%) respectively. Overall, we find that the highest contribution to total national CONUS methane
400 emissions occurs from facilities emitting in the 10-100 kg/hr range at 42% (37 - 46%). In terms of facility counts,
401 from the 673,940 total active oil/gas facilities we estimate in the CONUS for 2021, we estimate that essentially all
402 (i.e., ~99.9%) of these facilities emit methane below 100 kg/hr.

403 Our facility-level model estimates total methane emissions from US upstream/midstream oil/gas emissions
404 for 2021 to be 14.6 (12.7 - 16.8) Tg/yr, or 1,668,000 (1,453,000 – 1,921,000) kg/hr (Fig. 4), which corresponds to a
405 gross gas production normalized loss rate of 2.4%, assuming a uniform 80% methane content in natural gas across
406 oil/gas producing regions in the CONUS. This national emission total of 14.6 (12.7 - 16.8) Tg/yr is more than
407 double the EPA Greenhouse Gas Inventory Report for natural gas and petroleum systems in 2021, excluding post-
408 meter and distribution methane emissions (Inventory of U.S. Greenhouse Gas Emissions and Sinks, 2024). We
409 compare our total national estimates to previous estimates by seven studies that predominantly utilize satellite-based
410 remote-sensing platforms such as GOSAT and TROPOMI inversions (Lu et al., 2022, 2023; Maasackers et al.,
411 2021; Shen et al., 2022; Worden et al., 2022) except for Alvarez et al. (2018) and Omara et al. (2024) who developed
412 unique facility-based modeling approaches using empirical measurement data collected from multiple oil/gas basins
413 in the CONUS (Fig. 4). Our estimate of national methane emissions overlaps with six out of seven other national
414 estimates of oil/gas methane emissions for the US, with a combined average of 13.1 (ranging from 11.1 - 15.7)
415 Tg/yr. We do not estimate methane emissions from gathering/transmission/distribution pipelines, post-meter
416 emissions, abandoned oil and gas wells, and refineries due to the scarcity of measurement-based data for these
417 sources. Total methane emissions from these sources emit ~2 Tg/year of methane emissions based on other studies
418 (Williams et al., 2021; Alvarez et al., 2018; Omara et al., 2024; Weller et al., 2020; Inventory of U.S. Greenhouse
419 Gas Emissions and Sinks, 2024). Overall, our total national estimate of CONUS methane emissions for 2021 shows

420 good agreement with multiple independent and recent measurement-based estimates.



421

422 **Figure 4:** Comparison of total CONUS oil/gas emissions for 2021 from this facility-level measurement-based
 423 inventory compared to empirical estimates from other studies. Bars are colored according to the methodology used
 424 to derive the total national estimates, and the years within the bars represent the corresponding time periods for the
 425 estimates. Black inset lines represent 95% confidence intervals. Our total estimates for “This work” do not include
 426 emissions from other oil/gas methane sources such as abandoned oil and gas wells,
 427 transmission/gathering/distribution pipelines, post-meter emissions, and refineries. Emission estimates from Omara
 428 et al. (2024) do not include methane emissions from abandoned oil and gas wells. We assume that the remote
 429 sensing estimates (i.e., GOSAT and TROPOMI) include all oil/gas methane sources, including downstream
 430 emissions.

431

432 3.2 Distribution of emission rates at the basin-level scale

433

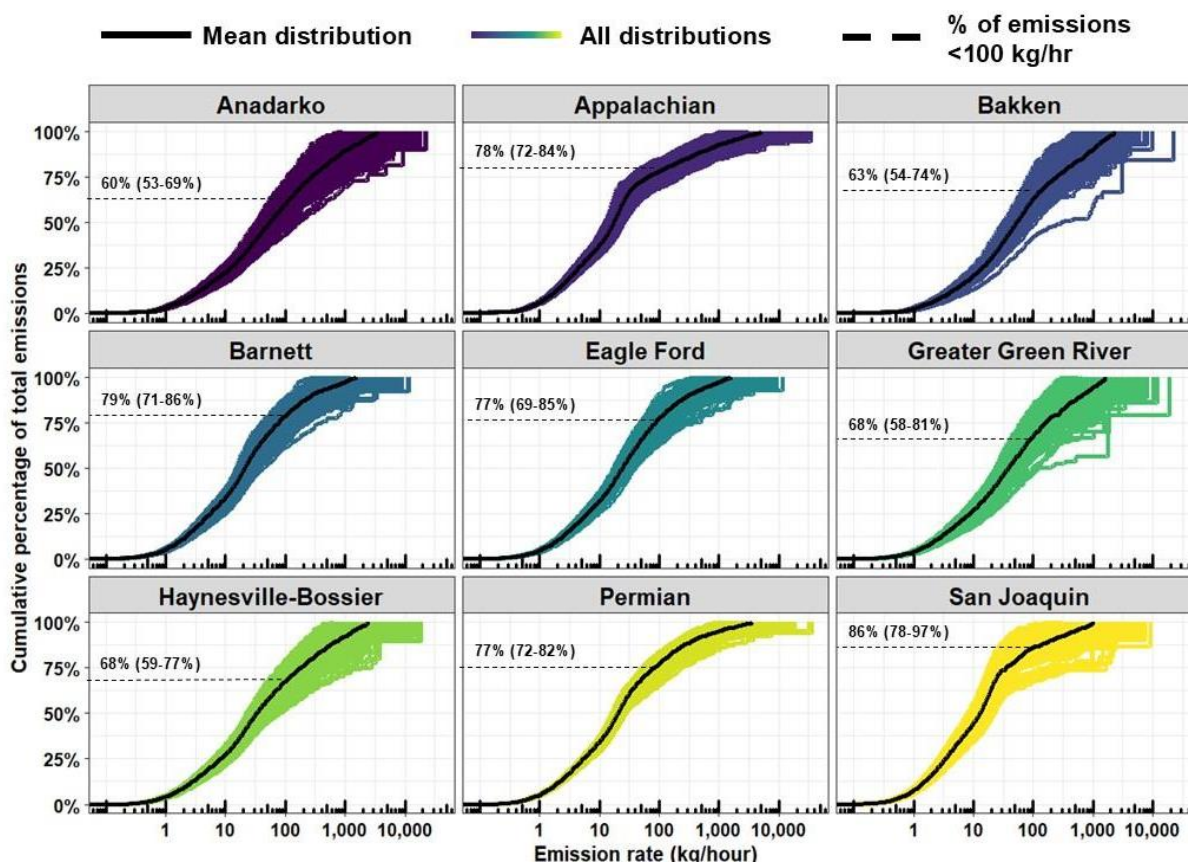
434 Among the top nine emitting oil/gas basins in the CONUS, we observe variations among the different
 435 basins in terms of the methane emission distributions, especially at higher emission rate thresholds (Fig. 5). The
 436 majority of the top nine emitting oil/gas basins in Fig. 5 show higher percentage contributions from facilities
 437 emitting <100 kg/hr when compared to our national estimate of 70% (61 – 81%) (Fig. 3). These percentage
 438 contributions vary from ~80% in the Permian, Appalachian, and Eagle Ford basins, up to ~90% in the oil-dominant
 439 San Joaquin basin. Only the Anadarko and Bakken basins have notably lower contributions to total emissions at the
 440 100 kg/hr threshold at ~60% compared to the national level, which is still a significant majority of total methane
 441 emissions. Despite these variations, our facility-level model estimates that the majority of total national oil/gas
 442 emissions are consistently contributed from facilities emitting <100 kg/hr for the top nine emitting basins.

443 Our estimated facility-level emission distributions for the top nine emitting oil/gas basins all follow an S-
444 shaped curve (Fig. 5) like the national distribution (Fig. 3), albeit with certain variations. For all basins, the initial
445 plateau in the emissions distribution curves ends at around 1 kg/hr before beginning to rise more steeply. For the
446 Appalachian and San Joaquin basins, the second plateau is at the 20-50 kg/hr emission rate threshold (Fig. 5). For
447 the remaining basins, the rise in the emission distribution curves plateaus gradually, indicating a more consistent
448 relationship of emission rate thresholds to their contribution to total emissions. The variability displayed among the
449 500 basin-level simulations differs among the oil/gas basins, with less spread in the 500 estimated methane
450 emissions distributions for the Appalachian, Anadarko, and Permian basins compared to the Uinta, Denver-
451 Julesburg, and San Joaquin basins (Fig. 5 and Fig. S6). These variations are likely caused in part by the overall total
452 basin-level methane emissions, where an extremely high estimated methane emission rate would have a greater
453 impact on the percentage contribution to the total for basins with lower overall emissions (e.g., the apparent outliers
454 for the Greater Green River and Bakken basins in Fig. 5). We discuss below other plausible causes for basin-to-
455 basin variability in the estimated methane emission distributions.

456 In terms of total methane emissions, the top two emitting oil/gas basins are the Permian and Appalachian,
457 which collectively account for 5.2 (4.4 – 6.3) Tg/year (Fig. S1) or 37% of total upstream and midstream oil/gas
458 methane emissions. This exceeds the cumulative contribution from the other seven highest emitting oil/gas basins
459 which collectively account for 3.7 (2.9 – 5.0) Tg/yr. Notably, we find that the highest emissions in the CONUS
460 occur from regions outside of any basin boundary 4.3 (1.2 – 6.3) Tg/year. Our estimates for basin-level total
461 emissions also show good agreement with remote-sensing satellite-based observations (Fig. S1), except for the
462 Appalachian, Bakken, Greater Green River, and Denver-Julesburg basins where our results are consistently more
463 than double those from the remote-sensing studies that used a prior-emission based inversion result (Lu et al., 2023;
464 Shen et al., 2022). These four basins are in regions with relatively low TROPOMI observation counts and densities
465 compared to other regions in the CONUS (Shen et al., 2022), in addition to other factors that could influence
466 satellite-based inversions such as the presence of many non-oil/gas sources such as coal, livestock, and landfills.
467 Overall, our estimates of total basin-level emissions are consistent with satellite-based observations.

468

469



470

471 **Figure 5:** A) Results from 500 model simulations showing the cumulative methane emissions distribution curves for
 472 total upstream/midstream oil/gas methane emissions for the top nine emitting oil/gas basins in the CONUS for 2021.
 473 The model averages for each basin are shown in solid black lines. Inset dashed lines represent the percentage
 474 contributions of total emission from sources emitting <100 kg/hr. Emission distribution curves for the remaining
 475 eleven oil/gas basins in the CONUS are shown in Fig. S6, and a map of the spatial boundaries used for the different
 476 oil/gas basins is shown in Fig. S10.

477

478 3.3 Distribution of emission rates by facility category

479

480 We find significant variations in the methane emission rate distribution curves among the different facility
 481 categories (Fig. 6A). Over 50% of total methane emissions from low (i.e., <15 boe/day, or <0.13 kt of methane
 482 production per year and non-low production well sites, lit flares, and G&B compressor stations occur from facilities
 483 emitting <100 kg/hr (Fig. 6A). In contrast, only 17% (15-18%) of emissions from processing plants, 19% (18-20%)
 484 of emissions from T&S compressor stations, and 9% (7-12%) of emissions from unlit flares are contributed from
 485 emission sources <100 kg/hr. Similar variability is also observed at other emission rate thresholds, such as only 1%
 486 (0-2%) of total emissions for T&S compressor stations, unlit flares, and processing plants originating from facilities
 487 emitting at rates <10 kg/hr, compared to 50% (43-58%) from low producing well sites and 30% (24-35%) from non-
 488 low producing well sites (Fig. 6A). At higher emission rate thresholds, we find that 33% (20-45%) of total emissions
 489 from T&S compressors and processing plants are emitted from facilities <200 kg/hr, compared to 84% (68-93%)

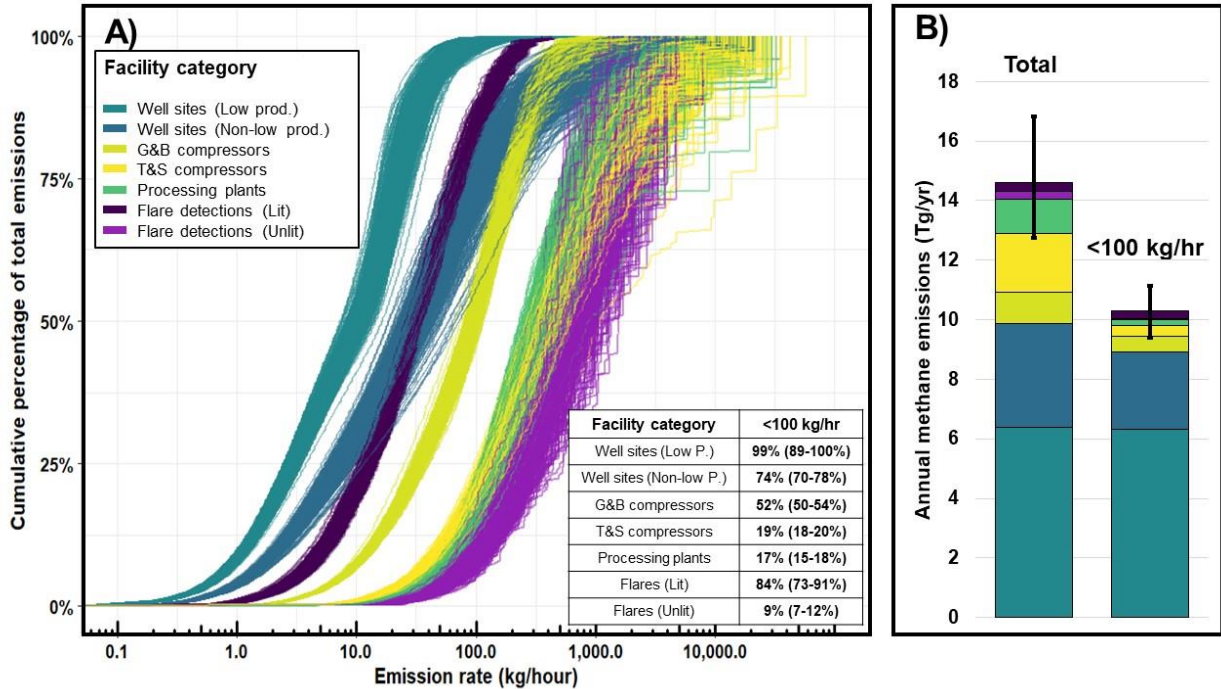
490 from non-low producing well sites (>boe/day of combined oil and gas), 86% (83-88%) from VIIRS flare detections,
491 78% (70-86%) from G&B compressor stations, and essentially 100% of emissions from low producing well sites.

492 A breakdown of the 673,940 total facilities in our model has 541,970 as low-producing well sites, followed
493 by 121,824 non-low-production well sites, 4,431 G&B compressor stations 2,093 T&S compressor stations, 919
494 processing plants, and 3,153 total VIIRS flare detections. Of these 673,940 total facilities, 99.5% (99.4 – 99.6%)
495 emit methane at rates <100 kg/hr (Fig. S11), and in turn contribute 70% of total methane emissions (Fig. 3). Overall,
496 we estimate that 68% of total CONUS oil/gas methane emissions for 2021 come from production well sites, of
497 which 44% are from low-production well sites with combined oil/gas production <15 boe/day (i.e., <0.13 kt of
498 methane production per year), and the remaining 24% from non-low production well sites (i.e., >15 boe/day) (Fig.
499 6B). Midstream facilities contribute 29% of total methane emissions, with 13% from T&S compressors, 8% from
500 processing plants, 7% from G&B compressor stations. The remaining 4% from VIIRS flare detections are evenly
501 split with 2% each from lit and unlit flares respectively. Based on the population counts for each facility category
502 and their corresponding total methane emissions, the average methane emission rate per facility category is highest
503 for processing plants at 146 (115 – 283) kg/hr, followed by 106 (89 – 129) kg/hr for T&S compressor stations, 27
504 (25 - 29) kg/hr for G&B compressor stations, 3.3 (2.9 – 3.8) kg/hr for non-low producing well sites, and 1.3 (1.2 –
505 1.5) kg/hr for low producing well sites. For VIIRS flares detections, we find a large difference in average emissions
506 between lit flares at 11 (9.2 – 13) kg/hr and unlit flares at 205 (132 – 294) kg/hr.

507 Production well sites constitute the bulk of total methane emissions among the facility categories we
508 considered, with most of these emissions contributed from low production well sites. Overall, we find that 67-90%
509 of well site emissions originated from only 10% of national oil and gas production in 2021 (Fig. S7), highlighting a
510 disproportionately large fraction of emissions relative to production. In terms of individual well site level production
511 values, the same 67-90% of total cumulative methane emissions were contributed from well sites producing >50
512 boe/day (i.e., 0.43 kt of methane production per year) or lower. For well sites producing 15 boe/day (i.e., 0.13 kt of
513 methane production per year) or lower, which is the production threshold used to define a well site as being
514 marginally producing in previous work (Deighton et al., 2020; Omara et al., 2022), we find that these low producing
515 well sites accounted for 50-75% of total well site emissions, or 4.7-6.8 Tg/yr.

516

517



518

519 **Figure 6:** A) Results from an ensemble of 500 estimated methane emission distributions showing the percentage of
 520 total methane emissions among facility categories contributed from facilities emitting at rates below an emission rate
 521 threshold. The inset table on the bottom right displays the discrete percentage contributions to total methane
 522 emissions contributed from facilities emitting <100 kg/hr. B) Breakdown of total annual methane emissions
 523 contributed from all emitting facility categories and those emitting at rates <100 kg/hr.

524

525 3.4 Comparisons to aerial remote sensing studies

526

527 We perform comparisons of the percentage contributions of methane emissions from facilities emitting
 528 below discrete emission rate thresholds between seven aerial remote sensing campaigns across four distinct regions
 529 and our estimated facility-level results (Fig. 7). The aerial remote sensing technologies include data from Bridger
 530 GML measurements (Kunkel et al., 2023; Xia et al., 2024), MethaneAIR (Omara et al. 2024; Miller et al. 2023), and
 531 the results from Global Airborne Observatory and next-generation Airborne Visible/Infrared Imaging Spectrometer
 532 campaigns (Cusworth et al., 2022) which are also included in the aerial detections used by Sherwin et al. (2024). In
 533 comparing the percentage contributions to total emissions from low-emitting sources between our facility-level
 534 estimates and the aerial remote sensing campaigns, we find that emission contributions agree well across aerial
 535 remote sensing campaigns for the total percentage of methane emissions from facilities emitting, as seen in Fig. 7
 536 for both less than 100 kg/hr and 200 kg/hr.

537 For the Bridger GML remote sensing campaigns (Kunkel et al., 2023; Xia et al., 2024), we find good
 538 agreement in the percentage of total emissions contributed from facilities emitting <200 and <100 kg/hr compared to
 539 our facility-level model estimates (Fig. 7). A comparison of continuous emissions distribution curves between our

540 facility-level emission distributions and two Bridger GML aerial remote sensing campaigns (Kunkel et al., 2023;
541 Xia et al., 2024) targeting four oil/gas basins is shown in Fig. S3. The Bridger GML aerial sampling platform has the
542 lowest LOD among the aerial campaigns we analyze in this work and a similar source resolution (i.e., 30 meters) to
543 our facility-level model (i.e., 50 meters), allowing for a more detailed comparison of continuous emission
544 distribution curves due to the higher number of detected methane sources at low emission rates provided by Bridger
545 GML surveys. We find close agreement between our facility-level methane emission distribution curves and the
546 observed emissions by Bridger GML in the four-basin aggregate provided by Xia et al. (2024) (Fig. S3A) which
547 includes Anadarko, Bakken, Eagle Ford and Permian basins (individual basin data are not currently available in Xia
548 et al. (2024)), as well as separately for the Permian remote sampling campaign (Fig. S3B) by Kunkel et al. (2023),
549 with the measured emissions from the Bridger GML surveys overlapping with our facility-level model simulations
550 throughout the continuous distribution of methane emission rates.

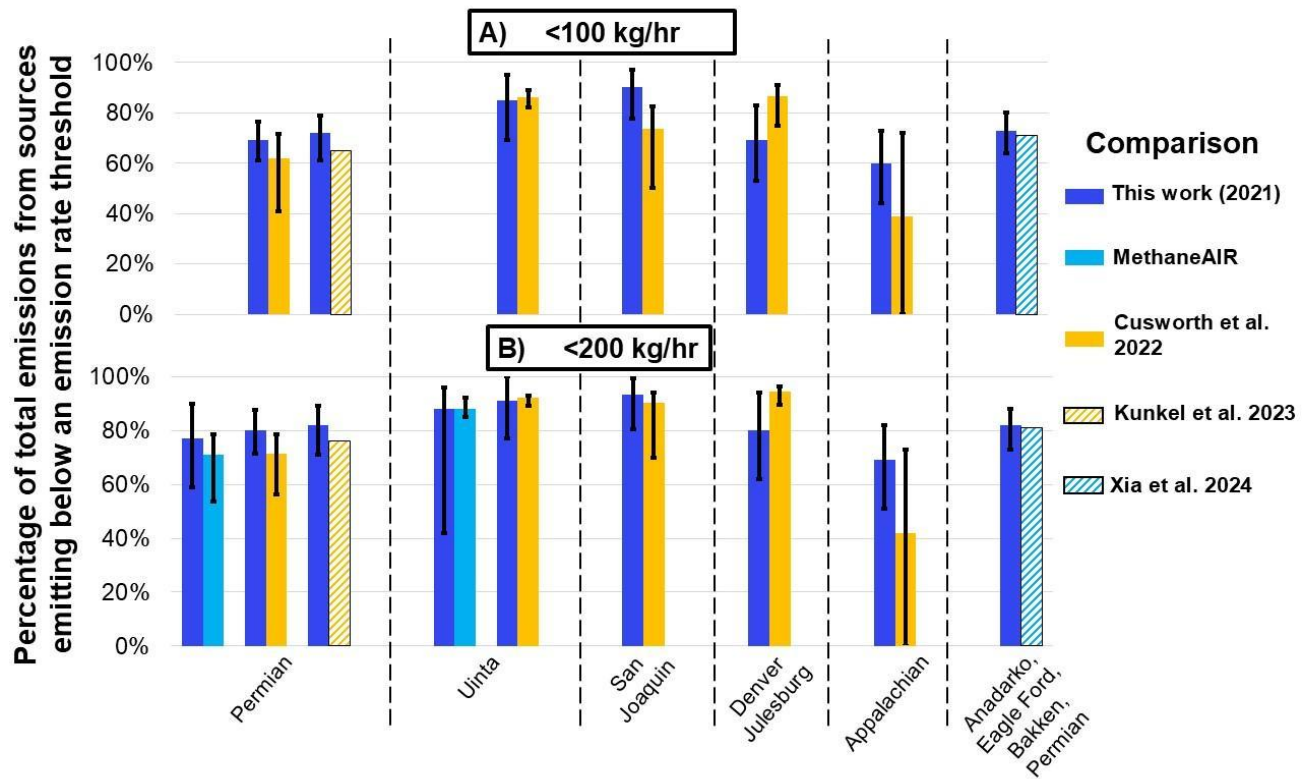
551 For the multiple aerial remote sensing campaigns performed by Cusworth et al. (2022), we generally find
552 good agreement with all of our estimates statistically overlapping for discrete emissions rate thresholds of <100
553 kg/hr and <200 kg/hr for the Permian and Uinta oil/gas basins (Fig. 7). For the San Joaquin and Denver-Julesburg
554 oil/gas basins, we see good agreement at the emission rate threshold of <200 kg/hr and at <100 kg/hr (i.e.
555 overlapping uncertainty bounds). For the Appalachian basin, we find broad agreement at both emission rate
556 thresholds of <100 kg/hr and <200 kg/hr, with our results consistently showing a 20-30% greater contribution from
557 emission sources below the discrete emission rate thresholds (Fig. 7). We find the closest agreement in the Permian
558 and Uinta oil/basins, where the differences in the average percentage contributions vary from -9% to +4% across the
559 three discrete emission rate thresholds of <100 and <200 kg/hr (Fig. 7). In Denver-Julesburg and Appalachian
560 basins, the differences are observed to be larger, compared to other basins, where the differences in average
561 percentage contributions across the discrete emission thresholds vary from -30% to +18%, however, they are within
562 our estimated uncertainty bounds. The detected point sources by Cusworth et al. (2022) in the Denver-Julesburg and
563 Appalachian basins contain many non-oil/gas point sources (Table S4), which may lead to additional uncertainty in
564 the comparisons for these basins since we use the relative proportions of point sources to subtract an estimated
565 contribution of non-oil/gas point sources from the TROPOMI estimates to provide a more direct comparison
566 between our estimates (since our study only focuses on upstream and midstream oil and gas sectors) and those of
567 Cusworth et al. (2022). Notably, the Appalachian basin contains the highest percentage contribution of non-oil/gas
568 point sources at 67% (Table S4). In contrast, we note that all of the detected point sources by Cusworth et al. (2022)
569 in the Permian and Uinta basins were attributed to oil/gas point sources (Table S4).

570 Our comparisons to the available flight results from MethaneAIR, which quantifies both total regional
571 methane emissions and high-emitting point sources >200 kg/hr from the same aerial platform (Chulakadabba et al.,
572 2023), show close agreement between our facility-level estimates and the available aerial campaigns in the Uinta
573 and Permian basins for facilities emitting <200 kg/hr (Fig. 7B). For the MethaneAIR flight in the Uinta basin, we
574 estimate that 92% (46 - 100%) of total oil/gas methane emissions are from sources emitting <200 kg/hr, compared to
575 88% from MethaneAIR (Fig. 7B). For the available flight in the Permian basin from MethaneAIR, we estimate total

576 contributions from sources emitting <200 kg/hr at 77% (59 – 90%) compared to the 71% estimated by MethaneAIR
 577 (Fig. 7B).

578 Overall, our findings show that our facility-level estimates closely agree with the results from multiple
 579 aerial remote sensing campaigns from different regions and using various measurement methods.

580



581

582 **Figure 7:** Comparisons of the cumulative percentage of oil/gas methane emissions from all oil/gas facilities emitting
 583 A) <100 kg/hr, and B) <200 kg/hr, between our facility-level empirical emissions estimates and aerial remote
 584 sensing campaigns. Bars are colored according to the study and grouped according to the target oil/gas basin(s). All
 585 results from the facility-level simulations (i.e., this work) are constrained to the spatial boundaries of the aerial
 586 campaigns for direct comparisons (note that for a given basin, spatial boundaries might be slightly different).
 587 Uncertainty bars for the facility-level simulations are the 2.5th and 97.5th percentiles of 500 simulations. Maps of all
 588 spatial boundaries used for comparisons are provided in Fig. S2. Comparisons to MethaneAIR are not performed at
 589 the <100 kg/hr threshold because MethaneAIR detections are not available for point sources below this emission
 590 rate threshold.

591

592 **4 Discussion**

593

594 Understanding how facilities with different magnitudes of emissions contribute to total regional emissions
595 has direct policy implications for methane quantification and mitigation, such as the selection of
596 measurement/screening methods with the appropriate detection sensitivities (Ravikumar et al., 2018). Our main
597 finding is that 70% of total oil/gas methane emissions from the upstream/midstream sectors come from facilities
598 emitting at rates <100 kg/hr, which is the emission rate threshold above which point source emissions are referred
599 to as “super-emitting” oil/gas source by the EPA (Standards of Performance for New, Reconstructed, and Modified
600 Sources and Emissions Guidelines for Existing Sources: Oil and Natural Gas Sector Climate Review, 2024). While
601 detecting and mitigating emissions from super emitters are important (Cusworth et al., 2022; Duren et al., 2019;
602 Sherwin et al., 2024), our results underscore the need to account for oil/gas methane sources emitting at lower rates,
603 as the cumulative contribution of lower-emitting sites accounts for a large majority of emissions across US oil/gas
604 basins. Facility-level, measurement-based data collected in other countries present a similar story. From a sample of
605 sites (n=302) measured via Bridger GML remote sensing platform in British Columbia, Canada (Tyner and Johnson,
606 2021), roughly 60% of the total quantified oil/gas site-level emissions originate from sites emitting <32 kg/hr. In
607 Romania, a site-level measurement-based inventory (Stavropoulou et al., 2023) using 178 measurements finds that
608 oil production facilities emitting <100 kg/hr contribute 78% of total oil/gas methane emissions in the studied region.
609 In short, the high percentage contribution from lower-emitting (<100 kg/hr) oil/gas facilities that account for a large
610 majority of total emissions is not unique to the US and is likely present in other countries as well. A combination of
611 approaches that characterize entire emission distributions across populations of sites (i.e., not just focusing on
612 measuring super-emitters) and quantification of regional-level emissions is needed in other countries to quantify the
613 relative contributions of low-emitting sources that in aggregate can be significant sources of overall oil/gas methane
614 emissions. Most of our analysis centers around quantifying the percentage contributions of oil/gas methane sources
615 emitting below one discrete emission rate threshold (i.e., <100 kg/hr, per EPA’s definition of a super-emitter). We
616 estimate that over 99% of the total oil/gas facilities that we analyze in this work emit below 100 kg/hr (Fig. S11),
617 which in turn contribute 70% (61 – 81%) of total methane emissions (Fig. 3). The emission rate threshold of 100
618 kg/hr is relevant to US policy decisions (EPA’s Final Rule for Oil and Natural Gas Operations Will Sharply Reduce
619 Methane and Other Harmful Pollution., 2024), but we also illustrate the importance of a complete characterization of
620 emissions, which gains importance as newer methane monitoring technologies have different LODs. For example,
621 the effective LOD at high probabilities of detection for available point source imaging satellites of ~200 kg/hr
622 (Jacob et al., 2022) would only be able to quantify 21% (10-32%) of all oil/gas point sources in the CONUS, if the
623 full oil/gas sector was mapped in its entirety, based on our facility-level results. When considering the relationship
624 of facility-level emission rates to total cumulative methane emissions, we find that oil/gas methane emissions in the
625 CONUS are dominated by many low-emitting facilities, which relates directly to methane measurement
626 technologies.

627 Point source-focused remote sensing platforms offer the advantage of rapidly surveying large areas (i.e.,
628 100’s-1,000’s km²) which facilitates the detection and quantification of high-emitting point sources (Cusworth et al.,
629 2022; Duren et al., 2019; Sherwin et al., 2024). In contrast, logistical constraints often limit the sample sizes for
630 ground-based vehicle sampling platforms, however, these limitations can be overcome with stratified random,

631 representative sampling and statistical analysis approaches like this work. Ground-based measurement platforms
632 provide much lower LODs (i.e., <1 kg/hr) when compared to remote sensing platforms, which are necessary to
633 quantify emissions from the large number of small methane sources we find that contribute roughly three-quarters of
634 total regional oil/gas emissions in the CONUS and will only improve as additional ground-based measurements are
635 gathered. Overall, our main findings highlight the importance of methods that can rapidly locate the small number of
636 high-emitting point sources we estimate, but our findings emphasize the need to account for the disproportionately
637 large majority percentage of total regional oil/gas emissions that are emitted from smaller diffuse methane sources.

638 When extrapolating our facility-level model results to the basin-level we see variations among the emission
639 distribution curves for different oil/gas basins, but still find that most methane emissions come from facilities
640 emitting <100 kg/hr. The variations in the emission distribution curves for different basins are driven by many
641 factors, such as the: production characteristics, number and density of facilities, different types and relative counts of
642 facility categories, the availability of empirical measurement data used to model emissions, and the total oil/gas
643 methane emissions (i.e., the denominator). For example, the Appalachian basin is dominated by a high number of
644 older low-production well sites (Deighton et al., 2020; Riddick et al., 2019; Enverus, 2024) with fewer midstream
645 facilities such as processing plants and G&B compressors, which contrasts with the Bakken basin where we find a
646 high number of midstream facilities, high-producing well sites, and VIIRS flare detections (Elvidge et al., 2015;
647 Enverus, 2024). When comparing the emissions distribution curves for the Bakken and Appalachian basins (Fig. 5),
648 we observe higher contributions from lower-emitting facilities for the Appalachian compared to the Bakken. An
649 example of differences in basin-level production is shown in Fig. S4 and Fig. S5, where we see variable profiles
650 among the different oil and gas-producing basins in terms of well site production characteristics, which are the main
651 source of total methane emissions in this work (Fig. 6). We also observe the influence of total basin-level emissions
652 on the variability among our emission distribution curves, where large emitting sources in the San Joaquin basin can
653 lead to high variability among the estimated emission distribution curves compared to the Permian basin which has
654 roughly ten times the total emissions compared to the San Joaquin (Fig. 5). We note that a direct comparison of our
655 model results with aerial remote sensing methods may be limited, in part, by methodological differences in methane
656 quantification approaches (and underlying uncertainties). The remote sensing observations assessed here as
657 snapshots may capture facility-level emission distributions that are not well represented in annually averaged
658 methane emissions distributions, as we estimate here. Nevertheless, we find broad agreement with these independent
659 aerial remote sensing estimates at the basin scale and across smaller spatial domains, as discussed. Ultimately, as
660 many characteristics will influence methane emissions distribution curves among different oil/gas producing regions
661 in the CONUS, mitigation strategies will need to be structured accordingly to the region they are targeting.

662 Our results find that over half of cumulative methane emissions from three different facility categories
663 come from facilities emitting <100 kg/hr, including methane emissions from lit and unlit flares. We show how the
664 large contributions from small methane sources to total regional emissions are not unique to any one facility
665 category, but it is important to contextualize our emission distribution curves with the corresponding total regional
666 emissions. Our facility-level estimates find that the main source of oil/gas methane emissions in the CONUS are

667 oil/gas production well sites, of which the low production category is responsible for 44% (39 – 49%) of the total
668 estimated oil/gas methane emissions in the CONUS in 2021. Low-producing well sites, also known as “marginal
669 wells”, have been shown in previous work to be a significant source of methane emissions, especially relative to
670 their contribution to overall oil/gas production (Deighton et al., 2020; Omara et al., 2022). Omara et al. (2022) found
671 that marginal wells contributed anywhere from 37%-75% of total methane emissions from production well sites,
672 which is like our estimates (i.e., 50-75%). Despite low production well sites having a lower mean emission rate
673 compared to other facility categories, the large facility counts result in significant aggregate total emissions of
674 methane. This implies that detection and mitigation strategies to reduce methane emissions from these and other
675 low-emitting oil and gas infrastructure (e.g., abandoned oil/gas wells) would require alternative mitigation and
676 detection approaches compared to those for the small number of super-emitting emission sources. For detection,
677 measurement methods that can measure emission rates between 0.1-100 kg/hr are required, since this range makes
678 up 70% of total methane emissions (Figure 3 and Table S1) as modeled herein. In terms of methane mitigation
679 policy, financial incentives, like the USD 4.7 billion from the Biden Bipartisan Infrastructure Law for abandoned
680 wells, could be used to prioritize the repair of old and leak-prone production well sites, as these low-producing well
681 sites only account for a small fraction (i.e., 5.6% in 2019) of total oil/gas production (Omara et al., 2022).

682 We see good agreement between our facility-level results and a majority of aerial remote sensing studies, which
683 are expected to capture a wide range of high-emitting facilities in a survey region. For example, when comparing
684 our model results to Kunkel et al. (2023) and Xia et al. (2024) we find that our estimated methane emissions closely
685 match the distribution of methane emissions measured in Bridger GML surveys (Fig. S3). We also find good
686 agreement to satellite remote sensing estimates of emissions, such as our basin-level (Fig. S1) and national-level
687 comparison to satellite inversions (Fig. 3), and other aerial remote sensing study regions (Table S2). Our
688 comparisons of the contributions of low-emitting sources below discrete emission rate thresholds also agree closely
689 with recent MethaneAIR, Kairos Aerospace, GAO, and AVIRIS-NG aerial surveys, whose results also highlight the
690 importance of small methane sources to overall oil/gas methane emissions. Recently, Sherwin et al. (2024)
691 suggested that a majority of total emissions originate from a small fraction of high-emitting sites. Notably, most of
692 the aerial measurements that are used in Sherwin et al. (2024) are obtained from the Cusworth et al. (2022) study,
693 with which we see good agreement (Fig. 7). Sherwin et al. (2024) perform an alternative analysis than Cusworth et
694 al. (2022) for aeri ally measured sources with <3 overpasses and assume that sources with one or two overpasses
695 emit at their observed intermittency of 100%, 50%, or 0% of the time. This difference in analytical approaches
696 produces higher contributions from aerial emissions in Sherwin et al. (2024) by 31% on average for seven aerial
697 campaigns compared to Cusworth et al. (2022) (Table S7), which uses a resampling approach described earlier in
698 the Methods Section 2.4. In addition, emissions from Sherwin et al. (2024) that are below aerial detection limits are
699 estimated using a combination of an equipment-level bottom-up model presented in Rutherford et al. (2021) for
700 production well sites, and emission factors from the U.S. Greenhouse Gas Inventory (Inventory of U.S. Greenhouse
701 Gas Emissions and Sinks, 2024) for midstream facilities, which produces 52% lower emissions on average for seven
702 aerial campaigns (Table S7). Therefore, the aeri ally measured emissions in Sherwin et al. (2024) are higher and the
703 emissions below aerial detection limits are lower which leads to a higher contribution to total methane emissions

704 from high-emitting facilities (Table S7). Ultimately, the broad agreement we find across multiple disparate
705 measurement techniques and platforms across Bridger GML aerial campaigns (Kunkel et al., 2023; Xia et al., 2024),
706 MethaneAIR measurements (MethaneAIR L4 Area Sources 2021 | Earth Engine Data Catalog, 2024; Omara et al.,
707 2024), and the multiple surveyed regions presented in Cusworth et al. (2022), altogether provide collective evidence
708 about the large contribution of smaller emission sources to total regional emissions.

709 Given the variability in methane detection technologies, a range of approaches can be taken to estimate methane
710 emission rate distributions, each providing unique advantages and disadvantages. MethaneAIR provides a novel
711 remote sensing approach where high-emitting point sources, distributed area sources and total regional emissions are
712 quantified using the same aerial platform, providing the ability to directly measure high-emitting point source and
713 diffuse area contributions to total regional estimates. In the work by Xia et al. (2024) they combine measurements
714 from Bridger GML across four oil/gas basins and use component-level simulations to account for facilities emitting
715 below the 3 kg/hr LOD of Bridger GML. Other approaches also exist, such as Cusworth et al. (2022) who combine
716 TROPOMI inversions to estimate total regional methane emissions with point source emissions quantified from their
717 aerial detection platforms (i.e., GAO, AVIRIS-NG). Similarly, Sherwin et al. (2024) combine point source emissions
718 measured via aerial remote sensing with site/facility-level emission rates estimates calculated from a combination of
719 an equipment-level bottom-up model for production well sites (Rutherford et al., 2021) and emission factors from the
720 2023 GHGI for midstream facilities (Inventory of U.S. Greenhouse Gas Emissions and Sinks, 2024) for facilities
721 emitting below aerial detection limits. Remote sensing studies have key advantages over ground-based sampling
722 platforms, such as rapidly surveying wide areas and capturing higher-emitting point sources, but have variable LODs
723 depending on the target region, topography, measurement technology, presence of co-located non-oil/gas methane
724 sources (i.e., source attribution), weather conditions, infrastructure density, and infrastructure type(s). These variables
725 pose additional challenges when quantifying the contributions from facilities emitting above/below specific emission
726 rate thresholds, which are critical information to inform mitigation policy. Assessing performance, tracking mitigation,
727 and accurate reporting requires building a comprehensive picture of emissions by characterizing all emitters big and
728 small, and reconciling with total basin/sub-basin level emissions. Ultimately, the key seems to be merging the best
729 data from both approaches to build a hybrid inventory, ideally using a multi-tiered system with multiple methods that
730 span a range of LODs that allow for gathering empirical measurements from facilities emitting at all parts of the
731 methane emission distribution curve. Our study is a step in that direction considering measurement-based data while
732 presenting a robust comparison with available independent remote sensing measurements. At the same time, large-
733 area aggregate emissions data obtained from wide-area remote sensing mapping or mass balance surveys can better
734 constrain total regional emissions (e.g. Cusworth et al. 2022; Omara et al. 2024) towards a more empirically robust
735 denominator in characterizing the relative contributions of small emission and high emission sources to total
736 emissions.

737 We show that our facility-level emission models produce national- and basin-level methane emissions estimates
738 that are in good agreement with other independent measurement-based studies. However, we note the following
739 limitations/biases that could be improved with future data collection efforts. The empirical measurements that we

740 use in our model are representative of the year and time they were measured (i.e., 2010-2020), meaning that they
741 would not reflect any updates in regulatory practices or changes in facility operational and emission management
742 practices. In addition, there are variations in the number of production well site empirical measurements among
743 oil/gas basins (Table S3) although a sensitivity analysis shows that excluding data from individual oil/gas basins
744 does not significantly impact our results (Fig. S9). Furthermore, there are several oil/gas methane emission sources
745 that we do not account for in our estimates, which include: gathering/transmission/distribution pipelines, oil refining
746 and transportation, abandoned oil/gas wells, offshore oil/gas infrastructure, post-meter sources, and oil/gas
747 distribution infrastructure in urban areas. For some sources omitted in this work such as abandoned oil/gas wells,
748 their inclusion would likely lead to a higher contribution from low-emitting facilities, since the highest recorded
749 emission rate from an abandoned oil/gas well is 76 kg/hr (Riddick et al., 2024). For others such as oil refineries,
750 their inclusion would likely lead to a lower contribution from small methane sources given their low facility counts
751 and high per-site emissions (Duren et al., 2019). Despite their omissions, total methane emissions from these sources
752 are currently estimated to account for 5-10% (Alvarez et al., 2018; Riddick et al., 2024; Inventory of U.S.
753 Greenhouse Gas Emissions and Sinks, 2024; Williams et al., 2021) of total oil/gas sectoral emissions. Our estimates
754 also utilize empirically measured emission rates from ground-based sampling platforms which are limited in
755 number, especially in the case of processing plants (n=20) and T&S compressor stations (n=50) (Table S2). The
756 empirical data used in our analysis includes a smaller sample of super-emitting facilities relative to those captured
757 by remote sensing platforms (Duren et al., 2019; Sherwin et al., 2024), but our use of production-normalized loss
758 rates and lognormal distributions to estimate facility-level methane emission rates anticipates and accounts for the
759 possibility of finding low-probability, high-magnitude emissions that occur at rates beyond those that appear in our
760 dataset of empirical observations. For example, our highest empirical emission rate is 1,360 kg/hr for a T&S
761 compressor station, whereas our maximum estimated facility-level emission rate across all 500 facility-level
762 emission distribution curves averages 7,500 kg/hr (3,000 - 21,000 kg/hr). Finally, we include a small number (i.e.,
763 5% of total empirical data used in the model) of measurements for production well-sites gathered using ground-
764 based component/source-level sampling methods from two studies (Deighton et al., 2020; Riddick et al., 2019). All
765 measurements from these two studies targeted the lowest production cohort of production well sites and exhibited
766 statistically lower emission rates than those gathered using facility-level ground-based methods for the same well
767 site production cohort, meaning that any bias introduced by the inclusion of these measurements would lead towards
768 the underestimation of total emissions and/or the percentage contributions from low-emitting sources. Despite these
769 limitations, we have shown that our results are broadly in agreement with satellite- and aerial-based remote sensing
770 studies at national/basin/local scales, and other facility-level estimates.

771 Going forward, several approaches can be used to better understand the percentage contributions from facilities
772 emitting at different leak rate thresholds, and ultimately improve our understanding of oil/gas methane emissions in
773 the CONUS and around the world. A combination of multiple satellite and aerial remote sensing approaches and
774 synthesis of their data by bringing in point source detections at multiple thresholds at the same time characterizing
775 total regional emissions as demonstrated using a compilation of multi-scale measurements seems a viable pathway
776 towards building a more complete picture of the overall methane emissions. Combining aerial and satellite remote

777 sensing measurements with ground-based site/facility-level estimates presents itself as an effective next step, as
778 implemented/suggested by prior studies (Allen, 2014; Alvarez et al., 2018). Aerial or satellite remote sensing
779 platforms focused on point source detection offer the ability to rapidly locate the small number of the highest
780 emitting facilities that contribute a disproportionate fraction of emissions, offering valuable data on specific facility
781 locations that allow for rapid mitigation. However, more direct observational approaches are needed to acquire total
782 emissions data which according to this study is dominated by small-emitting sources that are undetected by high-
783 emitting point source detection systems. Facility-level population-based approaches can account for the lower-
784 emitting facilities that contribute the most total oil/gas methane emissions, which is needed for accurate emission
785 reporting and understanding the contributions of total emissions above/below emission rate thresholds. The ground-
786 based estimates can be further constrained by large-area aggregated emission quantification provided by regional
787 remote sensing or mass balance mapping approaches (Shen et al., 2022; Omara et al., 2024; Jacob et al., 2022)
788 towards producing a more robust overall emission quantification.

789 **5 Conclusions**

790 In conclusion, our work highlights several key aspects of oil/gas methane emission rate distribution curves
791 in the CONUS for 2021, which include:

- 792 1. A large majority (70%) of total national continental oil/gas methane emissions in the US originate from
793 lower-emitting facilities (<100 kg/hr).
- 794 2. Emission rate distributions vary among different oil/gas basins, but among the top nine producing basins
795 we consistently find that most methane emissions (60%-86%) originate from oil/gas facilities emitting at
796 rates <100 kg/hr.
- 797 3. Production well sites were found to be responsible for 70% of regional oil/gas methane emissions, from
798 which the sites that accounted for only 10% of national oil and gas production in 2021, disproportionately
799 accounted for 67-90% of the total well site emissions.
- 800 4. Our results were consistently found to be in close agreement with those from independent aerial/satellite
801 remote sensing estimates, both in comparing contributions from discrete emission rate thresholds and
802 continuous emissions distribution curves, which emphasize the importance of the large majority
803 contribution of small-emitting methane sources to total oil/gas methane emissions.

804 Our results highlight, and quantify, the significant contributions of the large number of low-emitting oil/gas
805 facilities to total regional/basin/local oil/gas methane emissions in the CONUS for 2021. In addition to the CONUS,
806 the small oil/gas methane sources are likely a significant component of total regional emissions in other countries as
807 well as recent data suggest from Romania and Canada (Stavropoulou et al., 2023; Tyner and Johnson, 2021) and
808 would need to be further investigated to build a comprehensive assessment of small-emitting methane emissions and
809 their relative contributions to total oil/gas methane emissions globally. This work emphasizes the need for multi-

810 scale approaches to quantify total regional oil/gas methane emissions; and at the same time characterize and account
811 for the large contribution from small emission sources dispersed across a wide area, in addition to incorporating data
812 on high-emitting point sources towards producing overall robust methane emission quantification.

813
814 **Data availability**

815 All 500 full emission rate distributions at the national level are available to download from Zenodo (link:
816 <https://doi.org/10.5281/zenodo.13314532>). All estimated methane emission rate distributions at the basin or small
817 target scale are available upon request. Empirical measurement data used in the estimation of the methane emission
818 distribution curves are available from the references listed in Table S2.

819
820 **Code availability**

821 R code used to create the methane emission distribution curves and figures is available upon reasonable request.

822
823 **Acknowledgements**

824 We acknowledge funding support from the Bezos Earth Fund. We would like to thank Jack Warren and Luis Guanter
825 for their valuable efforts in analyzing point source emissions from MethaneAIR aerial campaigns.

826
827 **Author contributions**

828 JPW and RG designed this study. JPW created the code used to produce all results, with inputs from MO, KM, DZA,
829 and AH. MethaneAIR analysis was provided by JB, MS, and SW. Multi-sensor airborne intercomparison was
830 performed by JPW and RG. JPW prepared the manuscript with input from all co-authors.

831
832 **Competing interests**

833 The authors declare that they have no conflict of interest.

834
835 **References**

836 Allen, D. T.: Methane emissions from natural gas production and use: reconciling bottom-up and top-down
837 measurements, *Current Opinion in Chemical Engineering*, 5, 78–83, <https://doi.org/10.1016/j.coche.2014.05.004>,
838 2014.

839 Alvarez, R. A., Zavala-Araiza, D., Lyon, D. R., Allen, D. T., Barkley, Z. R., Brandt, A. R., Davis, K. J., Herndon, S.
840 C., Jacob, D. J., Karion, A., Kort, E. A., Lamb, B. K., Lauvaux, T., Maasackers, J. D., Marchese, A. J., Omara, M.,
841 Pacala, S. W., Peischl, J., Robinson, A. L., Shepson, P. B., Sweeney, C., Townsend-Small, A., Wofsy, S. C., and
842 Hamburg, S. P.: Assessment of methane emissions from the U.S. oil and gas supply chain, *Science*, 361, 186–188,
843 <https://doi.org/10.1126/science.aar7204>, 2018.

- 844 Enverus | Creating the future of energy together.: <https://www.enverus.com/>, last access: 25 March 2024.
- 845 Standards of Performance for New, Reconstructed, and Modified Sources and Emissions Guidelines for Existing
846 Sources: Oil and Natural Gas Sector Climate Review: <https://www.federalregister.gov/documents/2024/03/08/2024-00366/standards-of-performance-for-new-reconstructed-and-modified-sources-and-emissions-guidelines-for>, last
847 access: 22 July 2024.
- 849 AR6 Synthesis Report: Climate Change 2023: <https://www.ipcc.ch/report/ar6/syr/>, last access: 6 March 2024.
- 850 MethaneAIR L4 Area Sources 2021 | Earth Engine Data Catalog: [https://developers.google.com/earth-
851 engine/datasets/catalog/EDF_MethaneSAT_MethaneAIR_methaneair-L4area-2021](https://developers.google.com/earth-engine/datasets/catalog/EDF_MethaneSAT_MethaneAIR_methaneair-L4area-2021), last access: 27 March 2024.
- 852 Brandt, A. R., Heath, G. A., and Cooley, D.: Methane Leaks from Natural Gas Systems Follow Extreme Distributions,
853 *Environ. Sci. Technol.*, 50, 12512–12520, <https://doi.org/10.1021/acs.est.6b04303>, 2016.
- 854 Brantley, H. L., Thoma, E. D., Squier, W. C., Guven, B. B., and Lyon, D.: Assessment of Methane Emissions from
855 Oil and Gas Production Pads using Mobile Measurements, *Environ. Sci. Technol.*, 48, 14508–14515,
856 <https://doi.org/10.1021/es503070q>, 2014.
- 857 Caulton, D. R., Lu, J. M., Lane, H. M., Buchholz, B., Fitts, J. P., Golston, L. M., Guo, X., Li, Q., McSpirtt, J., Pan,
858 D., Wendt, L., Bou-Zeid, E., and Zondlo, M. A.: Importance of Superemitter Natural Gas Well Pads in the Marcellus
859 Shale, *Environ. Sci. Technol.*, 53, 4747–4754, <https://doi.org/10.1021/acs.est.8b06965>, 2019.
- 860 Chan Miller, C., Roche, S., Wilzewski, J. S., Liu, X., Chance, K., Souri, A. H., Conway, E., Luo, B., Samra, J.,
861 Hawthorne, J., Sun, K., Staebell, C., Chulakadabba, A., Sargent, M., Benmergui, J. S., Franklin, J. E., Daube, B. C.,
862 Li, Y., Laughner, J. L., Baier, B. C., Gautam, R., Omara, M., and Wofsy, S. C.: Methane retrieval from MethaneAIR
863 using the CO₂ Proxy Approach: A demonstration for the upcoming MethaneSAT mission, *EGUsphere*, 1–40,
864 <https://doi.org/10.5194/egusphere-2023-1962>, 2023.
- 865 Chen, Y., Sherwin, E. D., Berman, E. S. F., Jones, B. B., Gordon, M. P., Wetherley, E. B., Kort, E. A., and Brandt, A.
866 R.: Quantifying Regional Methane Emissions in the New Mexico Permian Basin with a Comprehensive Aerial Survey,
867 *Environ. Sci. Technol.*, 56, 4317–4323, <https://doi.org/10.1021/acs.est.1c06458>, 2022.
- 868 Chen, Y., Sherwin, E. D., Wetherley, E. B., Yakovlev, P. V., Berman, E. S. F., Jones, B. B., Hmiel, B., Lyon, D. R.,
869 Duren, R., Cusworth, D. H., and Brandt, A. R.: Reconciling ultra-emitter detections from two aerial hyperspectral
870 imaging surveys in the Permian Basin, 2024.
- 871 Chulakadabba, A., Sargent, M., Lauvaux, T., Benmergui, J. S., Franklin, J. E., Chan Miller, C., Wilzewski, J. S.,
872 Roche, S., Conway, E., Souri, A. H., Sun, K., Luo, B., Hawthorne, J., Samra, J., Daube, B. C., Liu, X., Chance, K.,
873 Li, Y., Gautam, R., Omara, M., Rutherford, J. S., Sherwin, E. D., Brandt, A., and Wofsy, S. C.: Methane point source
874 quantification using MethaneAIR: a new airborne imaging spectrometer, *Atmospheric Measurement Techniques*, 16,
875 5771–5785, <https://doi.org/10.5194/amt-16-5771-2023>, 2023.
- 876 Cusworth, D. H., Thorpe, A. K., Ayasse, A. K., Stepp, D., Heckler, J., Asner, G. P., Miller, C. E., Yadav, V., Chapman,
877 J. W., Eastwood, M. L., Green, R. O., Hmiel, B., Lyon, D. R., and Duren, R. M.: Strong methane point sources
878 contribute a disproportionate fraction of total emissions across multiple basins in the United States, *Proceedings of
879 the National Academy of Sciences*, 119, e2202338119, <https://doi.org/10.1073/pnas.2202338119>, 2022.
- 880 Deighton, J. A., Townsend-Small, A., Sturmer, S. J., Hoschouer, J., and Heldman, L.: Measurements show that
881 marginal wells are a disproportionate source of methane relative to production, *Journal of the Air & Waste
882 Management Association*, 70, 1030–1042, <https://doi.org/10.1080/10962247.2020.1808115>, 2020.
- 883 Duren, R. M., Thorpe, A. K., Foster, K. T., Rafiq, T., Hopkins, F. M., Yadav, V., Bue, B. D., Thompson, D. R.,
884 Conley, S., Colombi, N. K., Frankenberg, C., McCubbin, I. B., Eastwood, M. L., Falk, M., Herner, J. D., Croes, B. E.,
885 Green, R. O., and Miller, C. E.: California’s methane super-emitters, *Nature*, 575, 180–184,
886 <https://doi.org/10.1038/s41586-019-1720-3>, 2019.

- 887 Elvidge, C. D., Zhizhin, M., Baugh, K., Hsu, F.-C., and Ghosh, T.: Methods for Global Survey of Natural Gas Flaring
888 from Visible Infrared Imaging Radiometer Suite Data, *Energies*, 9, 14, <https://doi.org/10.3390/en9010014>, 2016.
- 889 ERG: City of Fort Worth Natural Gas Air Quality Study, Final Report, Eastern Research Group, Inc. (ERG), 2011.
- 890 Fox, T. A., Barchyn, T. E., Risk, D., Ravikumar, A. P., and Hugenholtz, C. H.: A review of close-range and screening
891 technologies for mitigating fugitive methane emissions in upstream oil and gas, *Environ. Res. Lett.*, 14, 053002,
892 <https://doi.org/10.1088/1748-9326/ab0cc3>, 2019.
- 893 Goetz, J. D., Floerchinger, C., Fortner, E. C., Wormhoudt, J., Massoli, P., Knighton, W. B., Herndon, S. C., Kolb, C.
894 E., Knipping, E., Shaw, S. L., and DeCarlo, P. F.: Atmospheric Emission Characterization of Marcellus Shale Natural
895 Gas Development Sites, *Environ. Sci. Technol.*, 49, 7012–7020, <https://doi.org/10.1021/acs.est.5b00452>, 2015.
- 896 de Gouw, J. A., Veefkind, J. P., Roosenbrand, E., Dix, B., Lin, J. C., Landgraf, J., and Levelt, P. F.: Daily Satellite
897 Observations of Methane from Oil and Gas Production Regions in the United States, *Sci Rep*, 10, 1379,
898 <https://doi.org/10.1038/s41598-020-57678-4>, 2020.
- 899 Jacob, D. J., Varon, D. J., Cusworth, D. H., Dennison, P. E., Frankenberg, C., Gautam, R., Guanter, L., Kelley, J.,
900 McKeever, J., Ott, L. E., Poulter, B., Qu, Z., Thorpe, A. K., Worden, J. R., and Duren, R. M.: Quantifying methane
901 emissions from the global scale down to point sources using satellite observations of atmospheric methane,
902 *Atmospheric Chemistry and Physics*, 22, 9617–9646, <https://doi.org/10.5194/acp-22-9617-2022>, 2022.
- 903 Johnson, M. R., Tyner, D. R., and Szekeres, A. J.: Blinded evaluation of airborne methane source detection using
904 Bridger Photonics LiDAR, *Remote Sensing of Environment*, 259, 112418, <https://doi.org/10.1016/j.rse.2021.112418>,
905 2021.
- 906 Kunkel, W. M., Carre-Burritt, A. E., Aivazian, G. S., Snow, N. C., Harris, J. T., Mueller, T. S., Roos, P. A., and
907 Thorpe, M. J.: Extension of Methane Emission Rate Distribution for Permian Basin Oil and Gas Production
908 Infrastructure by Aerial LiDAR, *Environ. Sci. Technol.*, 57, 12234–12241, <https://doi.org/10.1021/acs.est.3c00229>,
909 2023.
- 910 Lan, X., Talbot, R., Laine, P., and Torres, A.: Characterizing Fugitive Methane Emissions in the Barnett Shale Area
911 Using a Mobile Laboratory, *Environ. Sci. Technol.*, 49, 8139–8146, <https://doi.org/10.1021/es5063055>, 2015.
- 912 Lu, X., Jacob, D. J., Wang, H., Maasackers, J. D., Zhang, Y., Scarpelli, T. R., Shen, L., Qu, Z., Sulprizio, M. P.,
913 Nesser, H., Bloom, A. A., Ma, S., Worden, J. R., Fan, S., Parker, R. J., Boesch, H., Gautam, R., Gordon, D., Moran,
914 M. D., Reuland, F., Villasana, C. A. O., and Andrews, A.: Methane emissions in the United States, Canada, and
915 Mexico: evaluation of national methane emission inventories and 2010–2017 sectoral trends by inverse analysis of
916 in situ (GLOBALVIEWplus CH₄ ObsPack) and satellite (GOSAT) atmospheric observations, *Atmospheric Chemistry
917 and Physics*, 22, 395–418, <https://doi.org/10.5194/acp-22-395-2022>, 2022.
- 918 Lu, X., Jacob, D. J., Zhang, Y., Shen, L., Sulprizio, M. P., Maasackers, J. D., Varon, D. J., Qu, Z., Chen, Z., Hmiel,
919 B., Parker, R. J., Boesch, H., Wang, H., He, C., and Fan, S.: Observation-derived 2010–2019 trends in methane
920 emissions and intensities from US oil and gas fields tied to activity metrics, *Proceedings of the National Academy of
921 Sciences*, 120, e2217900120, <https://doi.org/10.1073/pnas.2217900120>, 2023.
- 922 Maasackers, J. D., Jacob, D. J., Sulprizio, M. P., Scarpelli, T. R., Nesser, H., Sheng, J., Zhang, Y., Lu, X., Bloom, A.
923 A., Bowman, K. W., Worden, J. R., and Parker, R. J.: 2010–2015 North American methane emissions, sectoral
924 contributions, and trends: a high-resolution inversion of GOSAT observations of atmospheric methane, *Atmospheric
925 Chemistry and Physics*, 21, 4339–4356, <https://doi.org/10.5194/acp-21-4339-2021>, 2021.
- 926 Miller, S. M., Wofsy, S. C., Michalak, A. M., Kort, E. A., Andrews, A. E., Biraud, S. C., Dlugokencky, E. J.,
927 Eluszkiewicz, J., Fischer, M. L., Janssens-Maenhout, G., Miller, B. R., Miller, J. B., Montzka, S. A., Nehr Korn, T.,
928 and Sweeney, C.: Anthropogenic emissions of methane in the United States, *Proceedings of the National Academy of
929 Sciences*, 110, 20018–20022, <https://doi.org/10.1073/pnas.1314392110>, 2013.
- 930 Mitchell, A. L., Tkacik, D. S., Roscioli, J. R., Herndon, S. C., Yacovitch, T. I., Martinez, D. M., Vaughn, T. L.,
931 Williams, L. L., Sullivan, M. R., Floerchinger, C., Omara, M., Subramanian, R., Zimmerle, D., Marchese, A. J., and

- 932 Robinson, A. L.: Measurements of Methane Emissions from Natural Gas Gathering Facilities and Processing Plants:
933 Measurement Results, *Environ. Sci. Technol.*, 49, 3219–3227, <https://doi.org/10.1021/es5052809>, 2015.
- 934 Nesser, H., Jacob, D. J., Maasackers, J. D., Lorente, A., Chen, Z., Lu, X., Shen, L., Qu, Z., Sulprizio, M. P., Winter,
935 M., Ma, S., Bloom, A. A., Worden, J. R., Stavins, R. N., and Randles, C. A.: High-resolution U.S. methane emissions
936 inferred from an inversion of 2019 TROPOMI satellite data: contributions from individual states, urban areas, and
937 landfills, *EGUsphere*, 1–36, <https://doi.org/10.5194/egusphere-2023-946>, 2023.
- 938 Ocko, I. B., Sun, T., Shindell, D., Oppenheimer, M., Hristov, A. N., Pacala, S. W., Mauzerall, D. L., Xu, Y., and
939 Hamburg, S. P.: Acting rapidly to deploy readily available methane mitigation measures by sector can immediately
940 slow global warming, *Environ. Res. Lett.*, 16, 054042, <https://doi.org/10.1088/1748-9326/abf9c8>, 2021.
- 941 Omara, M., Sullivan, M. R., Li, X., Subramanian, R., Robinson, A. L., and Presto, A. A.: Methane Emissions from
942 Conventional and Unconventional Natural Gas Production Sites in the Marcellus Shale Basin, *Environ. Sci. Technol.*,
943 50, 2099–2107, <https://doi.org/10.1021/acs.est.5b05503>, 2016.
- 944 Omara, M., Zimmerman, N., Sullivan, M. R., Li, X., Ellis, A., Cesa, R., Subramanian, R., Presto, A. A., and Robinson,
945 A. L.: Methane Emissions from Natural Gas Production Sites in the United States: Data Synthesis and National
946 Estimate, *Environ. Sci. Technol.*, 52, 12915–12925, <https://doi.org/10.1021/acs.est.8b03535>, 2018.
- 947 Omara, M., Zavala-Araiza, D., Lyon, D. R., Hmiel, B., Roberts, K. A., and Hamburg, S. P.: Methane emissions from
948 US low production oil and natural gas well sites, *Nat Commun*, 13, 2085, [https://doi.org/10.1038/s41467-022-29709-](https://doi.org/10.1038/s41467-022-29709-3)
949 3, 2022.
- 950 Omara, M., Himmelberger, A., MacKay, K., Williams, J. P., Benmergui, J., Sargent, M., Wofsy, S. C., and Gautam,
951 R.: Constructing a measurement-based spatially explicit inventory of US oil and gas methane emissions, *Earth System*
952 *Science Data Discussions*, 1–25, <https://doi.org/10.5194/essd-2024-72>, 2024.
- 953 Plant, G., Kort, E. A., Brandt, A. R., Chen, Y., Fordice, G., Gorchov Negron, A. M., Schwietzke, S., Smith, M., and
954 Zavala-Araiza, D.: Inefficient and unlit natural gas flares both emit large quantities of methane, *Science*, 377, 1566–
955 1571, <https://doi.org/10.1126/science.abq0385>, 2022.
- 956 Ravikumar, A. P., Wang, J., McGuire, M., Bell, C. S., Zimmerle, D., and Brandt, A. R.: “Good versus Good Enough?”
957 Empirical Tests of Methane Leak Detection Sensitivity of a Commercial Infrared Camera, *Environ. Sci. Technol.*, 52,
958 2368–2374, <https://doi.org/10.1021/acs.est.7b04945>, 2018.
- 959 Rella, C. W., Hoffnagle, J., He, Y., and Tajima, S.: Local- and regional-scale measurements of CH₄, δ¹³CH₄, and C₂H₆
960 in the Uintah Basin using a mobile stable isotope analyzer, *Atmospheric Measurement Techniques*, 8, 4539–4559,
961 <https://doi.org/10.5194/amt-8-4539-2015>, 2015.
- 962 Riddick, S. N., Mauzerall, D. L., Celia, M. A., Kang, M., Bressler, K., Chu, C., and Gum, C. D.: Measuring methane
963 emissions from abandoned and active oil and gas wells in West Virginia, *Science of The Total Environment*, 651,
964 1849–1856, <https://doi.org/10.1016/j.scitotenv.2018.10.082>, 2019.
- 965 Riddick, S. N., Ancona, R., Mbua, M., Bell, C. S., Duggan, A., Vaughn, T. L., Bennett, K., and Zimmerle, D. J.: A
966 quantitative comparison of methods used to measure smaller methane emissions typically observed from
967 superannated oil and gas infrastructure, *Atmospheric Measurement Techniques*, 15, 6285–6296,
968 <https://doi.org/10.5194/amt-15-6285-2022>, 2022.
- 969 Riddick, S. N., Mbua, M., Santos, A., Emerson, E. W., Cheptonui, F., Houlihan, C., Hodshire, A. L., Anand, A.,
970 Hartzell, W., and Zimmerle, D. J.: Methane emissions from abandoned oil and gas wells in Colorado, *Science of The*
971 *Total Environment*, 922, 170990, <https://doi.org/10.1016/j.scitotenv.2024.170990>, 2024.
- 972 Robertson, A. M., Edie, R., Snare, D., Soltis, J., Field, R. A., Burkhart, M. D., Bell, C. S., Zimmerle, D., and Murphy,
973 S. M.: Variation in Methane Emission Rates from Well Pads in Four Oil and Gas Basins with Contrasting Production
974 Volumes and Compositions, *Environ. Sci. Technol.*, 51, 8832–8840, <https://doi.org/10.1021/acs.est.7b00571>, 2017.

- 975 Robertson, A. M., Edie, R., Field, R. A., Lyon, D., McVay, R., Omara, M., Zavala-Araiza, D., and Murphy, S. M.:
 976 New Mexico Permian Basin Measured Well Pad Methane Emissions Are a Factor of 5–9 Times Higher Than U.S.
 977 EPA Estimates, *Environ. Sci. Technol.*, 54, 13926–13934, <https://doi.org/10.1021/acs.est.0c02927>, 2020.
- 978 Rutherford, J. S., Sherwin, E. D., Ravikumar, A. P., Heath, G. A., Englander, J., Cooley, D., Lyon, D., Omara, M.,
 979 Langfitt, Q., and Brandt, A. R.: Closing the methane gap in US oil and natural gas production emissions inventories,
 980 *Nat Commun*, 12, 4715, <https://doi.org/10.1038/s41467-021-25017-4>, 2021.
- 981 Shen, L., Gautam, R., Omara, M., Zavala-Araiza, D., Maasakkers, J. D., Scarpelli, T. R., Lorente, A., Lyon, D., Sheng,
 982 J., Varon, D. J., Nesser, H., Qu, Z., Lu, X., Sulprizio, M. P., Hamburg, S. P., and Jacob, D. J.: Satellite quantification
 983 of oil and natural gas methane emissions in the US and Canada including contributions from individual basins,
 984 *Atmospheric Chemistry and Physics*, 22, 11203–11215, <https://doi.org/10.5194/acp-22-11203-2022>, 2022.
- 985 Sherwin, E., Zhang, Z., Chen, Y., Wetherley, E. B., Yakovlev, P., Berman, E. S. F., Jones, B. B., Thorpe, A. K.,
 986 Ayasse, A. K., Duren, R., Brandt, A. R., and Cusworth, D. H.: Quantifying oil and natural gas system emissions using
 987 one million aerial site measurements, <https://doi.org/10.21203/rs.3.rs-2406848/v1>, 2023a.
- 988 Sherwin, E. D., Rutherford, J. S., Chen, Y., Aminfard, S., Kort, E. A., Jackson, R. B., and Brandt, A. R.: Single-blind
 989 validation of space-based point-source detection and quantification of onshore methane emissions, *Sci Rep*, 13, 3836,
 990 <https://doi.org/10.1038/s41598-023-30761-2>, 2023b.
- 991 Sherwin, E. D., Rutherford, J. S., Zhang, Z., Chen, Y., Wetherley, E. B., Yakovlev, P. V., Berman, E. S. F., Jones, B.
 992 B., Cusworth, D. H., Thorpe, A. K., Ayasse, A. K., Duren, R. M., and Brandt, A. R.: US oil and gas system emissions
 993 from nearly one million aerial site measurements, *Nature*, 627, 328–334, [https://doi.org/10.1038/s41586-024-07117-](https://doi.org/10.1038/s41586-024-07117-5)
 994 5, 2024.
- 995 Stavropoulou, F., Vinković, K., Kers, B., de Vries, M., van Heuven, S., Korbeń, P., Schmidt, M., Wietzel, J., Jagoda,
 996 P., Necki, J. M., Bartyzel, J., Maazallahi, H., Menoud, M., van der Veen, C., Walter, S., Tuzson, B., Ravelid, J.,
 997 Morales, R. P., Emmenegger, L., Brunner, D., Steiner, M., Hensen, A., Velzeboer, I., van den Bulk, P., Denier van
 998 der Gon, H., Delre, A., Edjabou, M. E., Scheutz, C., Corbu, M., Iancu, S., Moaca, D., Scarlat, A., Tudor, A., Vizireanu,
 999 I., Calcan, A., Ardelean, M., Ghemulet, S., Pana, A., Constantinescu, A., Cusa, L., Nica, A., Baciuc, C., Pop, C.,
 1000 Radovici, A., Mereuta, A., Stefanie, H., Dandocsi, A., Hermans, B., Schwietzke, S., Zavala-Araiza, D., Chen, H., and
 1001 Röckmann, T.: High potential for CH₄ emission mitigation from oil infrastructure in one of EU’s major production
 1002 regions, *Atmospheric Chemistry and Physics*, 23, 10399–10412, <https://doi.org/10.5194/acp-23-10399-2023>, 2023.
- 1003 Thorpe, M. J., Krieting, A., Altamura, D., Dudiak, C. D., Conrad, B. M., Tyner, D. R., Johnson, M. R., Brasseur, J.
 1004 K., Roos, P., Kunkel, W., Carre-Burritt, A., Abate, J., Price, T., Yarialian, D., Kennedy, B., Newton, E., Rodriguez,
 1005 E., Elfar, O. I., and Zimmerle, D. J.: Deployment-invariant probability of detection characterization for aerial LiDAR
 1006 methane detection, 2024.
- 1007 Tyner, D. R. and Johnson, M. R.: Where the Methane Is—Insights from Novel Airborne LiDAR Measurements
 1008 Combined with Ground Survey Data, *Environ. Sci. Technol.*, 55, 9773–9783, <https://doi.org/10.1021/acs.est.1c01572>,
 1009 2021.
- 1010 Inventory of U.S. Greenhouse Gas Emissions and Sinks: [https://www.epa.gov/ghgemissions/inventory-us-](https://www.epa.gov/ghgemissions/inventory-us-greenhouse-gas-emissions-and-sinks)
 1011 [greenhouse-gas-emissions-and-sinks](https://www.epa.gov/ghgemissions/inventory-us-greenhouse-gas-emissions-and-sinks), last access: 6 March 2024.
- 1012 EPA’s Final Rule for Oil and Natural Gas Operations Will Sharply Reduce Methane and Other Harmful Pollution.:
 1013 <https://www.epa.gov/controlling-air-pollution-oil-and-natural-gas-operations/epas-final-rule-oil-and-natural-gas>, last
 1014 access: 5 March 2024.
- 1015 Weller, Z. D., Hamburg, S. P., and von Fischer, J. C.: A National Estimate of Methane Leakage from Pipeline Mains
 1016 in Natural Gas Local Distribution Systems, *Environ. Sci. Technol.*, 54, 8958–8967,
 1017 <https://doi.org/10.1021/acs.est.0c00437>, 2020.
- 1018 Williams, J. P., Regehr, A., and Kang, M.: Methane Emissions from Abandoned Oil and Gas Wells in Canada and the
 1019 United States, *Environ. Sci. Technol.*, 55, 563–570, <https://doi.org/10.1021/acs.est.0c04265>, 2021.

1020 Williams, J. P., El Hachem, K., and Kang, M.: Controlled-release testing of the static chamber methodology for direct
1021 measurements of methane emissions, *Atmospheric Measurement Techniques*, 16, 3421–3435,
1022 <https://doi.org/10.5194/amt-16-3421-2023>, 2023.

1023 Worden, J. R., Cusworth, D. H., Qu, Z., Yin, Y., Zhang, Y., Bloom, A. A., Ma, S., Byrne, B. K., Scarpelli, T.,
1024 Maasackers, J. D., Crisp, D., Duren, R., and Jacob, D. J.: The 2019 methane budget and uncertainties at 1° resolution
1025 and each country through Bayesian integration Of GOSAT total column methane data and a priori inventory estimates,
1026 *Atmospheric Chemistry and Physics*, 22, 6811–6841, <https://doi.org/10.5194/acp-22-6811-2022>, 2022.

1027 Xia, H., Strayer, A., and Ravikumar, A. P.: The Role of Emission Size Distribution on the Efficacy of New
1028 Technologies to Reduce Methane Emissions from the Oil and Gas Sector, *Environ. Sci. Technol.*, 58, 1088–1096,
1029 <https://doi.org/10.1021/acs.est.3c05245>, 2024.

1030 Yacovitch, T. I., Herndon, S. C., Pétron, G., Kofler, J., Lyon, D., Zahniser, M. S., and Kolb, C. E.: Mobile Laboratory
1031 Observations of Methane Emissions in the Barnett Shale Region, *Environ. Sci. Technol.*, 49, 7889–7895,
1032 <https://doi.org/10.1021/es506352j>, 2015.

1033 Zhang, Y., Gautam, R., Pandey, S., Omara, M., Maasackers, J. D., Sadavarte, P., Lyon, D., Nesser, H., Sulprizio, M.
1034 P., Varon, D. J., Zhang, R., Houweling, S., Zavala-Araiza, D., Alvarez, R. A., Lorente, A., Hamburg, S. P., Aben, I.,
1035 and Jacob, D. J.: Quantifying methane emissions from the largest oil-producing basin in the United States from space,
1036 *Science Advances*, 6, eaaz5120, <https://doi.org/10.1126/sciadv.aaz5120>, 2020.

1037 Zhou, X., Yoon, S., Mara, S., Falk, M., Kuwayama, T., Tran, T., Cheadle, L., Nyarady, J., Croes, B., Scheehle, E.,
1038 Herner, J. D., and Vijayan, A.: Mobile sampling of methane emissions from natural gas well pads in California,
1039 *Atmospheric Environment*, 244, 117930, <https://doi.org/10.1016/j.atmosenv.2020.117930>, 2021.

1040 Zimmerle, D., Vaughn, T., Luck, B., Lauderdale, T., Keen, K., Harrison, M., Marchese, A., Williams, L., and Allen,
1041 D.: Methane Emissions from Gathering Compressor Stations in the U.S., *Environ. Sci. Technol.*, 54, 7552–7561,
1042 <https://doi.org/10.1021/acs.est.0c00516>, 2020.

1043

1044

1045

1046

1047

1048

1049

1050